

MAGII CAT II. GENERAL CHARACTERISTICS OF THE Mg II ABSORBING CIRCUMGALACTIC MEDIUM

NIKOLE M. NIELSEN¹, CHRISTOPHER W. CHURCHILL¹, AND GLENN G. KACPRZAK^{2,3}

Accepted for publication in ApJ, August 5, 2013

ABSTRACT

We examine the Mg II absorbing circumgalactic medium (CGM) for the 182 intermediate redshift ($0.072 \leq z \leq 1.120$) galaxies in the “Mg II Absorber-Galaxy Catalog” (MAGII CAT, Nielsen et al.). We parameterize the anti-correlation between equivalent width, $W_r(2796)$, and impact parameter, D , with a log-linear fit, and show that a power law poorly describes the data. We find that higher luminosity galaxies have larger $W_r(2796)$ at larger D (4.3σ). The covering fractions, f_c , decrease with increasing D and $W_r(2796)$ detection threshold. Higher luminosity galaxies have larger f_c ; no absorption is detected in lower luminosity galaxies beyond 100 kpc. Bluer and redder galaxies have similar f_c for $D < 100$ kpc, but for $D > 100$ kpc, bluer galaxies have larger f_c , as do higher redshift galaxies. The “absorption radius,” $R(L) = R_*(L/L_*)^\beta$, which we examine for four different $W_r(2796)$ detection thresholds, is more luminosity sensitive to the B -band than the K -band, more sensitive for redder galaxies than for bluer galaxies, and does not evolve with redshift for the K -band, but becomes more luminosity sensitive towards lower redshift for the B -band. These trends clearly indicate a more extended Mg II absorbing CGM around higher luminosity, bluer, and higher redshift galaxies. Several of our findings are in conflict with other works. We address these conflicts and discuss the implications of our results for the low-ionization, intermediate redshift CGM.

Subject headings: galaxies: halos — quasars: absorption lines

1. INTRODUCTION

Understanding the formation and evolution of galaxies is one of the foremost problems facing extragalactic research. Over the last decade, theoretical activity has been focused on studying how galaxies form and evolve in the context of the response of baryonic gas to dark matter halos of various masses and to physical processes such as stellar and AGN feedback (e.g., Birnboim & Dekel 2003; Maller & Bullock 2004; Kereš et al. 2005; Dekel & Birnboim 2006; Birnboim et al. 2007; Ocvirk, Pichon, & Teyssier 2008; Kereš et al. 2009; Oppenheimer et al. 2010; Stewart et al. 2011; van de Voort et al. 2011; van de Voort & Schaye 2012). These theoretical works have established that the circumgalactic medium (CGM) is a dynamic environment comprising inflowing accretion, outflowing winds, and gas that recycles between the halo and galaxy.

What has become clear is that the CGM is intimately linked to galaxy morphology, stellar populations and kinematics, and chemical evolution. The detailed physics governing the heating and cooling of baryonic gas regulates the formation and galactic-scale dynamical motions of stars, which in turn feedback and govern the physics of the gas in the CGM (e.g., Dekel & Silk 1986; Ceverino & Klypin 2009). Since this paradigm of galaxy evolution suggests a strong CGM-galaxy connection, many investigators have taken a phenomenological approach to developing models that predict the observable geometric distribution and kinematics of baryonic gas in and around galaxies (e.g., Weisheit 1978; Lanzetta & Bowen 1992; Charlton & Churchill 1996; Mo & Miralda-Escude 1996; Benjamin & Danly 1997; Charlton & Churchill 1998; Tinker & Chen 2008; Chelouche & Bowen 2010;

Bouché et al. 2012).

As such, the CGM is an astrophysical environment which, at any point in the evolution of a galaxy, yields clues to both its historical development and future evolution. Therefore, observations of the CGM around individual galaxies promise to provide highly sought constraints on the physics governing the global properties of galaxies. In practice, the CGM is almost exclusively accessible via absorption lines present in the spectra of background objects (traditionally using the technique of quasar absorption lines). Studying the CGM-galaxy connection is desirable over all redshifts, with the vast majority of work to date having been focused on $z \leq 1$ (however, cf., Adelberger et al. 2005; Simcoe et al. 2006; Steidel et al. 2010; Rudie et al. 2012). At these redshifts, galaxy photometric and spectral properties can be measured with relatively high accuracy and modest investment in telescope time with Mg II absorption (e.g., Bergeron & Boissè 1991; Steidel, Dickinson, & Persson 1994; Churchill et al. 2005; Chen et al. 2010a; Kacprzak et al. 2011c).

The Mg II $\lambda\lambda 2796, 2803$ doublet is especially well suited at intermediate redshifts since the absorption is observable in the optical. Furthermore, Mg II absorption is ideal for tracing low ionization, metal-enriched CGM gas in that it arises in a wide range of HI environments, from $\log N(\text{HI}) \simeq 16.5$ to greater than 21.5 (Bergeron & Stasińska 1986; Steidel & Sargent 1992; Churchill et al. 1999, 2000a; Rao & Turnshek 2000; Rigby, Charlton, & Churchill 2002). It is also well established that Mg II absorption probes key CGM structures such as outflow gas (e.g., Tremonti et al. 2007; Weiner et al. 2009; Martin & Bouché 2009; Rubin et al. 2010) and inflow gas (e.g., Ribaudo et al. 2011; Rubin et al. 2012; Thom et al. 2011; Kacprzak et al. 2012) associated with galaxies.

Through the efforts of the aforementioned studies, the behavior of Mg II CGM absorption in relation to various galaxy properties has been incrementally characterized over the last two decades. Examples of some of the findings include relationships between the strength of Mg II absorp-

¹ New Mexico State University, Las Cruces, NM 88003
nnielsen@nmsu.edu, cwc@nmsu.edu

² Swinburne University of Technology, Victoria 3122, Australia
gkacprzak@astro.swin.edu.au

³ Australian Research Council Super Science Fellow

tion and galaxy luminosity (Kacprzak et al. 2008; Chen et al. 2010a), galaxy mass (Bouché et al. 2006; Gauthier et al. 2009; Churchill et al. 2013b), star formation or specific star formation rate (Chen et al. 2010b; Ménard et al. 2011), galaxy color (Zibetti et al. 2007; Bordoloi et al. 2011), galaxy morphology (Kacprzak et al. 2007), and galaxy orientation (Bordoloi et al. 2011; Bouché et al. 2012; Kacprzak et al. 2011c; Kacprzak, Churchill, & Nielsen 2012; Churchill et al. 2013a).

Generally speaking, these investigations have yielded results that appear to be converging on an observational portrait of the Mg II absorbing CGM that is more or less consistent with the broad scenario forwarded by theory and simulations. For example, evidence is mounting that accretion may preferentially reside in a coplanar geometry (e.g., Steidel et al. 1997; Kacprzak et al. 2010; Stewart et al. 2011; Kacprzak et al. 2011c), whereas winds may outflow along the galaxy minor axis (Bordoloi et al. 2011; Bouché et al. 2012; Churchill et al. 2013a; Kacprzak, Churchill, & Nielsen 2012). However, due to the complex ionization structure, non-uniform metal enrichment, and dynamical processes of the CGM, and due to the wide range of galaxy properties, such as luminosity, color, mass, and morphology, the data exhibit substantial scatter. As such, while some works have found statistically significant correlations between two quantities or between combined/scaled quantities, many works have reported connections between galaxy and Mg II absorption CGM properties either based on general trends (i.e., correlations that are not statistically significant above the 3σ level) or on slight reductions in the scatter of certain relationships by combining/scaling one or more measured quantity.

We compiled the “Mg II Absorber-Galaxy Catalog” (MAGIIICAT) which is described in detail in Paper I of this series (Nielsen et al. 2013), with the aim to further illuminate the CGM-galaxy connection at higher statistical significance and over a wide range of galaxy properties. In this paper, we utilize the data to address several long-standing questions with regard to the Mg II CGM-galaxy connection. In § 2, we briefly describe the galaxy sample, which has uniform photometric properties and impact parameters for a Λ CDM cosmology ($H_0 = 70 \text{ km s}^{-1} \text{ Mpc}^{-1}$, $\Omega_M = 0.3$ and $\Omega_\Lambda = 0.7$). In § 3, we present an examination of (1) galaxy color and absolute magnitude evolution, (2) the dependence of $W_r(2796)$ on galaxy color, (3) the dependence of $W_r(2796)$ on impact parameter, (4) covering fraction as a function of impact parameter and $W_r(2796)$ for luminosity, color, and redshift subsamples, and (5) the luminosity scaling of “halo absorption radius” and the behavior of covering fraction with $W_r(2796)$, galaxy color, and redshift. In § 4, we discuss the implications of our results and give concluding remarks in § 5.

2. GALAXY SAMPLE AND SUBSAMPLES

From an exhaustive literature search, we compiled a catalog of galaxies with spectroscopic redshifts $0.07 \leq z \leq 1.1$ within a projected distance of $D \leq 200 \text{ kpc}$ from a background quasar, with known Mg II absorption or an upper limit on absorption less than 0.3 \AA . We distinguish between isolated and group galaxies, where group galaxies have a nearest neighbor within 100 kpc and have a velocity separation no greater than 500 km s^{-1} , and focus only on isolated galaxies in the present work. The total catalog consists of 182 isolated galaxies. Full details of all galaxies and Mg II absorption properties as well as the various selection methods used are presented in Paper I. Here we briefly describe the general properties of

MAGIIICAT.

The sample presented here comprises 182 isolated galaxies toward 134 sightlines, covering a redshift range $0.072 \leq z_{\text{gal}} \leq 1.120$, with a median of $\langle z \rangle = 0.359$. The impact parameter range is $5.4 \leq D \leq 194 \text{ kpc}$, with median $\langle D \rangle = 49 \text{ kpc}$.

For each galaxy, we determined rest-frame AB absolute magnitudes, M_B and M_K , by computing k -corrections appropriate for the observed magnitudes (e.g., Kim, Goobar, & Perlmutter 1996) using the extended Coleman et al. (1980) spectral energy distribution (SED) templates from Bolzonella et al. (2000). We selected a galaxy SED by comparing the observed galaxy colors to the redshifted SEDs. Luminosities, L_B/L_B^* and L_K/L_K^* , were obtained using a linear fit to M_B^* with redshift from Faber et al. (2007) (B -band) and using $M_K^*(z)$ as expressed in Eq. 2 from Cirasuolo et al. (2010) (K -band). Absolute B -band magnitudes range from $-16.1 \geq M_B \geq -23.1$, corresponding to luminosities of $0.02 \leq L_B/L_B^* \leq 5.87$, with median $L_B/L_B^* = 0.611$. Absolute K -band magnitudes range from $-17.0 \geq M_K \geq -25.3$, corresponding to $0.006 \leq L_K/L_K^* \leq 9.7$. Rest-frame $B-K$ colors range from $0.04 \leq B-K \leq 4.09$, with median $B-K = 1.48$. We obtain K -band absolute magnitudes and luminosities, and $B-K$ colors for all but 18 of the galaxies.

Galaxies in MAGIIICAT were bifurcated into several subsamples for analysis. When dividing the galaxy-absorber pairs into subsamples, we either took a sample driven approach by splitting the sample at the median value of a given observed quantity, or dividing the sample based upon historical precedent, such as $W_r(2796)$ cuts. The full sample was sliced by the median galaxy redshift, L_B/L_B^* , L_K/L_K^* , or $B-K$. Table 1 presents the characteristics of the full sample and each subsample, including the number of galaxies, the median value by which the catalog was cut, and the minimum, maximum, and mean values of galaxy redshift, B - and K -band luminosity, and $B-K$ color. The subsample names listed will be used throughout this paper.

3. RESULTS

In this section, we report on the luminous properties of the galaxies and directly compare them to the properties of the Mg II absorbing CGM. The analysis presented here is based upon direct observables. We do not scale or combine measured quantities. We also do not scale or fit the data to models of the CGM. Our aim is to characterize the Mg II CGM-galaxy connection directly with no assumptions and to provide information that can be directly interpreted in terms of primary observables. We examine only bivariate relationships, reserving further analysis, such as multivariate techniques for future work to appear in later papers of this series.

3.1. Galaxy Magnitudes, Luminosities, and Colors Versus Redshift

Since the CGM as probed by Mg II may depend upon galaxy stellar populations, and these populations are known to evolve, we examined whether the galaxy magnitudes and rest-frame colors evolve with redshift for the sample. A Kendall- τ rank correlation test yielded a 4.4σ significance that M_B correlates with z_{gal} (i.e., galaxies at higher redshift are brighter in the B -band), whereas M_K shows a weak trend for redshift evolution (2.2σ). Faber et al. (2007) found that M_B^* brightens with increasing redshift from the DEEP2+COMBO-17 surveys. The average M_B of the sample presented here increases with redshift more rapidly than M_B^* . Similarly, Cirasuolo et al.

TABLE 1
SUBSAMPLE CHARACTERISTICS

Subsample	# Gals	Cut ^a	z_{gal}			L_B/L_B^*			L_K/L_K^*			$B-K$		
			Min	Max	Mean	Min	Max	Mean	Min ^b	Max ^b	Mean ^b	Min ^b	Max ^b	Mean ^b
All	182	...	0.072	1.120	0.418	0.017	5.869	0.855	0.006	9.712	0.883	0.038	4.090	1.537
Low z	91	0.359	0.072	0.358	0.225	0.017	3.759	0.734	0.006	4.901	0.654	0.283	3.037	1.554
High z	91	0.359	0.359	1.120	0.612	0.071	5.869	0.976	0.016	9.712	1.123	0.038	4.090	1.520
Low L_B/L_B^*	91	0.611	0.072	0.941	0.411	0.017	0.610	0.306	0.006	1.680	0.271	0.038	4.090	1.410
High L_B/L_B^*	91	0.611	0.096	1.120	0.425	0.613	5.869	1.405	0.241	9.712	1.452	0.483	3.303	1.655
Low L_K/L_K^*	82	0.493	0.110	0.941	0.396	0.019	1.440	0.376	0.006	0.487	0.222	0.038	3.037	1.231
High L_K/L_K^*	82	0.493	0.096	1.017	0.410	0.189	5.869	1.359	0.499	9.712	1.544	0.637	4.090	1.843
Blue	82	1.482	0.098	1.017	0.444	0.019	3.522	0.803	0.006	2.602	0.454	0.038	1.478	1.047
Red	82	1.482	0.096	0.852	0.362	0.035	5.869	0.931	0.026	9.712	1.312	1.487	4.090	2.027

^a The median value by which each subsample was bifurcated. The cut is inclusive to the “high” bins and red bin.

^b Only including galaxies with a value for M_K .

(2010) found that M_K^* tends to brighten with increasing redshift from UKIDSS, whereas the average M_K of the sample presented here does not exhibit redshift evolution. As such, we may be seeing that galaxies associated with Mg II absorption or an upper limit on absorption are characterized by bluer colors at higher redshift. However, selection effects may be important. Virtually all the galaxies were selected or discovered (for a summary of the selection methods used, see Nielsen et al. 2013) using the red band in the observer frame, which probes further toward the B -band in the galaxy rest frame with increasing redshift. However, this cannot explain the lack of evolution in the K -band.

We also conducted a rank correlation test on galaxy luminosities versus redshift, z_{gal} , since we calculate the luminosities from the absolute magnitudes. In the B -band, we find no redshift evolution of L_B/L_B^* to the 1.2σ level. Similarly in the K -band, we find that L_K/L_K^* does not correlate with redshift at the 0.9σ level. The lack of correlations here are due to the fact that we take into account the redshift evolution of M_B^* from Faber et al. (2007) and M_K^* from Cirasuolo et al. (2010) in our luminosity calculations.

A rank correlation test on $B-K$ versus z_{gal} shows that the null hypothesis of no correlation can be ruled out to a confidence level (CL) no better than 1.8σ , indicating that the $B-K$ rest-frame color of galaxies in MAGIIICAT does not evolve with redshift. This result is consistent with Zibetti et al. (2007) who use statistical methods in which individual galaxies were not directly identified with absorbers for $0.4 \leq z \leq 1$ using observed g , r , i , and z band magnitudes for $W_r(2796) \geq 0.8 \text{ \AA}$. A direct comparison is difficult because we use optical B -band and $2.2 \mu\text{m}$ infrared (K -band) absolute magnitudes to determine rest-frame colors and we study systems with much smaller $W_r(2796)$ than represented by their sample. Slicing the sample presented here at $W_r(2796) = 0.8 \text{ \AA}$ to compare to the Zibetti et al. (2007) sample, we obtain 0.8σ for $W_r(2796) \geq 0.8 \text{ \AA}$ and for $W_r(2796) < 0.8 \text{ \AA}$ we obtain 1.7σ .

3.2. Galaxy Luminosities and Colors Versus $W_r(2796)$

To determine whether $W_r(2796)$ exhibits some dependency on galaxy luminosity, we performed a non-parametric Kendall’s τ rank correlation test that allows for upper limits on either the dependent or independent variable for bivariate data (see Brown, Hollander, & Korwar 1974; Wang & Wells 2000) with $W_r(2796)$ as the dependent variable. The null hy-

pothesis of no correlation could not be ruled out for $W_r(2796)$ against L_B/L_B^* (0.2σ), L_K/L_K^* (0.6σ), M_B (0.9σ), and M_K (0.5σ). The lack of correlations found here are interesting in view of the arguments by Bouché et al. (2006), who derive an anti-correlation between $W_r(2796)$ and galaxy luminosity with a dependence on the faint-end slope of the galaxy luminosity function and a proportionality between galaxy luminosity and the cross-section of the absorbing CGM.

To determine if $W_r(2796)$ has any dependency on galaxy color, we performed the non-parametric Kendall’s τ rank correlation test on $W_r(2796)$ against $B-K$. The test indicates that $W_r(2796)$ does not directly correlate with galaxy color for the full sample (1.3σ). A Kendall’s τ rank correlation test between $W_r(2796)$ and $B-K$ for the subsample with $D \leq 50$ kpc indicates that $W_r(2796)$ is also not correlated with color at smaller impact parameters (0.5σ).

The lack of a correlation between $W_r(2796)$ and $B-K$ is consistent with the findings of Chen et al. (2010a), who examined $B-R$ colors for $0.1 \leq z \leq 0.5$. However, the result is contrary to the statistically based results of Zibetti et al. (2007), who find bluer colors from the integrated light selected by stronger Mg II absorbers and redder colors selected by weaker absorbers for $0.4 \leq z \leq 1$, where the minimum $W_r(2796)$ of their sample is 0.8 \AA . A direct comparison with the work of Zibetti et al. (2007) is difficult due to its statistical nature. However, a Kendall’s τ test examining the $W_r(2796) \geq 0.8 \text{ \AA}$ subsample of MAGIIICAT yielded a slight trend between $W_r(2796)$ and $B-K$ (2.1σ) such that larger equivalent widths may show a weak trend with galaxy color. Bifurcating the full galaxy sample at $W_{\text{cut}} = 0.1, 0.3, 0.6$, and 1.0 \AA , we find a 2.5σ significance for a correlation between $W_r(2796)$ and $B-K$ for galaxies hosting $W_r(2796) \geq 1.0 \text{ \AA}$ absorption; for the very strongest absorbers, the redder the galaxy, the greater the Mg II equivalent width. As mentioned, this is contrary to the findings of Zibetti et al. (2007).

To examine the possible Mg II equivalent width distribution dependence on $B-K$ color, we also performed a Kolmogorov-Smirnov (KS) test comparing the cumulative $W_r(2796)$ distribution functions of red ($B-K \geq 1.48$) and blue ($B-K < 1.48$) galaxies. We limited the test to include only those galaxies with detected Mg II absorption. The two subsamples are statistically consistent with having been drawn from the same parent distribution ($\simeq 0.5 \sigma$). Limiting the sample to galaxies with $D \leq 50$ kpc, the KS test results remain below 1σ . Though the distribution for red galaxies has power beyond the

largest and smallest $W_r(2796)$ of the blue galaxies, the statistics do not ferret out a difference between the two galaxy subsamples; the average and maximum $W_r(2796)$ for $D \leq 50$ kpc associated with red galaxies and blue galaxies are consistent (average 1.02 and 0.92 Å, with maximum 2.9 and 2.3 Å, respectively).

Our findings that the $W_r(2796)$ distributions from the CGM within $D = 50$ kpc of blue and red galaxies are indistinguishable is at odds with the dramatic finding of Bordoloi et al. (2011). They report a factor of eight times larger equivalent width associated with blue galaxies compared to red galaxies in stacked spectra for which the CGM is probed within $D = 50$ kpc.

3.3. $W_r(2796)$ and Impact Parameter

A commonly known property of Mg II galaxies is the anti-correlation between $W_r(2796)$ and impact parameter, D , (e.g., Lanzetta & Bowen 1990; Bergeron & Boissè 1991; Steidel 1995; Bouché et al. 2006; Kacprzak et al. 2008; Chen et al. 2010a; Churchill et al. 2013a). In Figure 1, we present $W_r(2796)$ versus D . Galaxies with detected Mg II absorption are plotted as solid blue points and those with upper limits on absorption are plotted as open blue points with downward arrows.

We performed a non-parametric Kendall’s τ rank correlation test on $W_r(2796)$ against D , allowing for upper limits on $W_r(2796)$. For this sample, $W_r(2796)$ is anti-correlated with D at the 7.9 σ level. Since $W_r(2796)$ correlates with the number of clouds (Voigt profile components, Petitjean & Bergeron 1990; Churchill et al. 2003; Evans 2011), this result indicates that either the column densities, velocity spreads, or both, diminish with projected distance from the galaxy.

To parameterize the general behavior of the anti-correlation, we used the Expectation-Maximization maximum-likelihood method (Wolynetz 1979) accounting for upper limits on $W_r(2796)$ to fit a power law, $\log W_r(2796) = \alpha_1 \log D + \alpha_2$, and a log-linear fit, $\log W_r(2796) = \alpha_1 D + \alpha_2$, to the data. The data are poorly described by a power law [green, long dashed curve in Figure 1, from Chen et al. (2010a)] due to the substantial population of $W_r(2796) < 0.1$ Å absorbers and upper limits. We present the log-linear fit and its 1 σ uncertainties in Figure 1 (solid black curve) for $\alpha_1 = -0.015 \pm 0.002$ and $\alpha_2 = 0.27 \pm 0.11$.

The considerable scatter about this relation *may* suggest that $W_r(2796)$ is governed by physical processes related to the galaxy such as luminosity (cf., Kacprzak et al. 2008; Chen et al. 2010a), mass (cf., Bouché et al. 2006; Gauthier et al. 2009; Lundgren et al. 2009; Churchill et al. 2013b), star formation (cf., Chen et al. 2010b; Ménard et al. 2011), or orientation (cf., Bordoloi et al. 2011; Bouché et al. 2012; Kacprzak et al. 2011c; Kacprzak, Churchill, & Nielsen 2012; Churchill et al. 2013a). Alternatively, the CGM is inherently patchy (Churchill et al. 2007, 2013a).

To examine possible trends and/or sources of this scatter in the distribution of $W_r(2796)$ versus D , we applied the two-dimensional Kolmogorov-Smirnov (2DKS) test. This test examines if the 2D distribution of $W_r(2796)$ and D from two samples can be ruled out as being consistent.

We first investigated bifurcations of the full sample about the median values of $B-K$, z_{gal} , L_B/L_B^* , and L_K/L_K^* , which are presented in Figure 2. Performing a 2DKS test on the subsamples, we find that the null hypothesis that blue and red

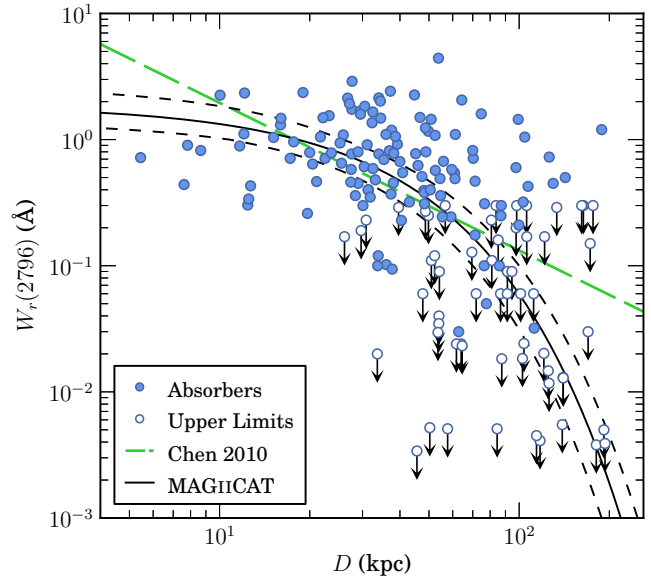


FIG. 1.— The Mg II $\lambda 2796$ rest-frame equivalent width, $W_r(2796)$, versus impact parameter, D . Galaxies with detected Mg II absorption are presented as solid blue points, whereas those with upper limits on absorption are open blue points with downward arrows. The full sample comprises 182 galaxies with a 7.9 σ anti-correlation between $W_r(2796)$ and D . The green, long dashed curve is the power law fit obtained by Chen et al. (2010a) for their data. The solid curve is a log-linear maximum likelihood fit to the data presented here, $\log W_r(2796) = \alpha_1 D + \alpha_2$, where $\alpha_1 = -0.015 \pm 0.002$ and $\alpha_2 = 0.27 \pm 0.11$. Short dashed curves provide 1 σ uncertainties in the fit.

galaxies are drawn from the same population can not be ruled out to the 1.6 σ level. Using a redshift cut, the data show a weak trend for larger $W_r(2796)$ at fixed D for high z galaxies (2.2 σ). A 2DKS test on the luminosities shows that high L_B/L_B^* and L_K/L_K^* are found with larger $W_r(2796)$ at fixed D than low luminosities at the 4.2 σ and 4.3 σ level, respectively. We then examined only galaxies with detected absorption in each subsample. In this case, the significance level decreases for all subsamples.

We also divided the sample into quartiles by $B-K$, z_{gal} , L_B/L_B^* , and L_K/L_K^* and performed the 2DKS test on the lowest and highest quartiles. We obtained $P(\text{KS}) = 0.03, 0.30, 0.0007$, and 0.0006 for $B-K$, z_{gal} , L_B/L_B^* , and L_K/L_K^* , respectively. At best, there is a 3.4 σ significance that the distribution or scatter of $W_r(2796)$ versus D is due to a dependence on L_K/L_K^* , a 3.4 σ significance of a connection to L_B/L_B^* , and a 2.1 σ significance it is connected to $B-K$. There is clearly no redshift dependence. When we examine only galaxies for which we have detectable absorption, we find that the significance level decreases or remains the same for all subsamples.

3.4. Covering Fraction and Impact Parameter

Here we examined the dependence of covering fraction directly on impact parameter and galaxy luminosity, color, and redshift. We present directly observable quantities, making no assumptions with regard to the Mg II absorbing CGM density profile or geometry.

3.4.1. Covering Fraction Within Fixed Impact Parameters

In order to examine the covering fraction within a fixed projected radial distance from the galaxies, we computed the quantity $f_{D_{\text{max}}} \equiv f(W \geq W_{\text{cut}}, D \leq D_{\text{max}})$, which we define as the fraction of absorbers with $W_r(2796) \geq W_{\text{cut}}$ inside a projected separation of D_{max} from the galaxy.

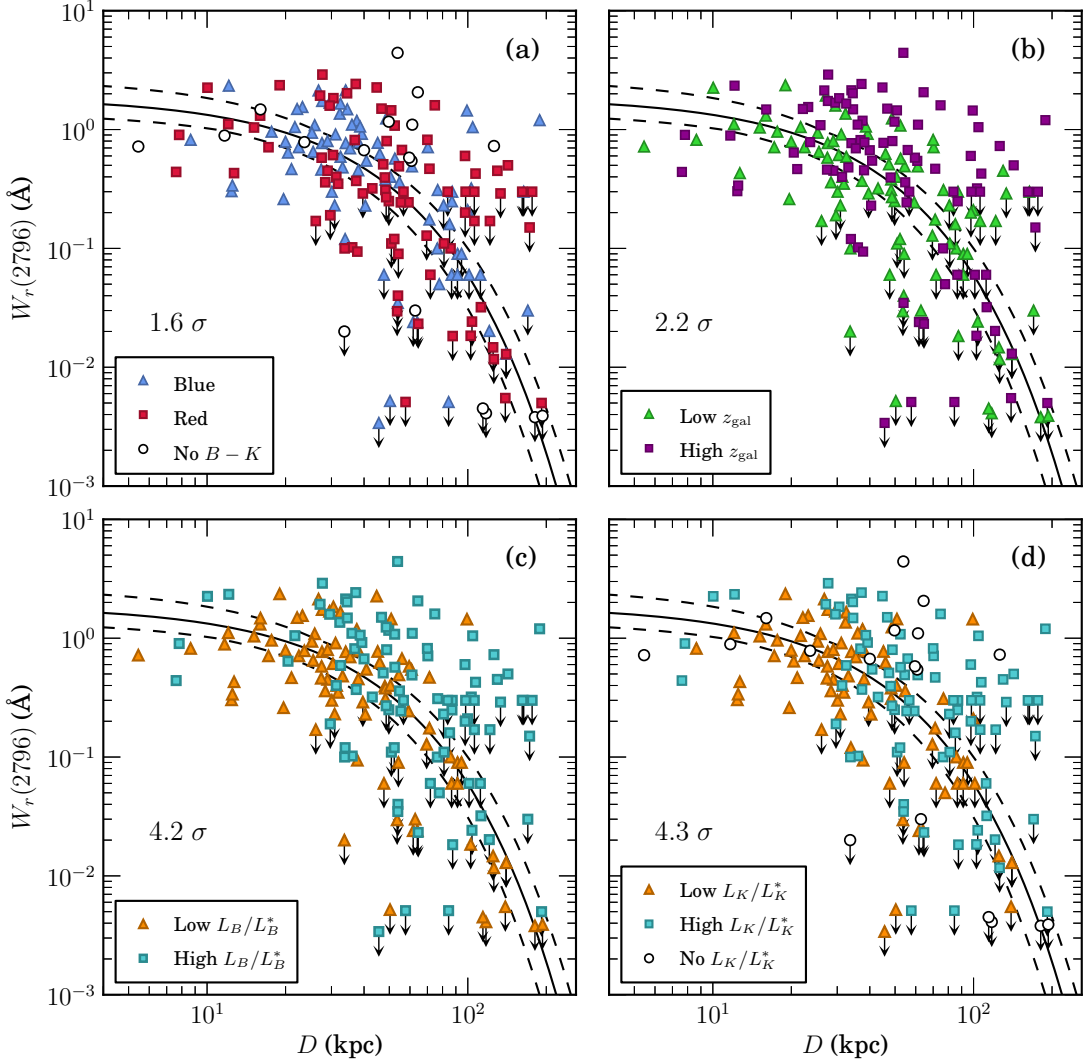


FIG. 2.— The Mg II equivalent width, $W_r(2796)$, as a function of impact parameter, D , split by median (a) galaxy color, (b) redshift, (c) B -band luminosity, and (d) K -band luminosity. Galaxies with no K -band magnitude are presented as open points in panels *a* and *d*. The null hypothesis that two subsamples are drawn from the same population can be ruled out to the 1.6σ ($B-K$), 2.2σ (z_{gal}), 4.2σ (L_B/L_B^*), and 4.3σ (L_K/L_K^*) level. The significance level decreases in all cases when we only consider galaxies for which we have detected Mg II absorption.

In Figure 3, we plot $f_{D_{\text{max}}}$ against D_{max} in 10 kpc intervals. The uncertainties in $f_{D_{\text{max}}}$ are shown as shaded regions. These are the upper and lower limits, calculated using the formalism for binomial statistics (see Gehrels 1986). Values of $f_{D_{\text{max}}}$ at $D_{\text{max}} \leq 10$ kpc are not robust given the small number of galaxies within this impact parameter⁴. Due to the relative undersampling of galaxies at $D_{\text{max}} > 150$ kpc and the cumulative nature of $f_{D_{\text{max}}}$, the covering fraction will be virtually unchanging outside this impact parameter; thus the shape of $f_{D_{\text{max}}}$ versus D_{max} is less robust for $D_{\text{max}} > 150$ kpc.

In Figure 3 (upper panels), we present $f_{D_{\text{max}}}$ for the full galaxy sample and for low and high luminosity galaxies. For each W_{cut} subsample, the covering fraction of the Mg II absorbing CGM inside $D = D_{\text{max}}$ decreases as D_{max} is increased. At a given D_{max} , there is a clear trend that as W_{cut} is increased, $f_{D_{\text{max}}}$ decreases, indicating that the covering fraction

⁴ Of the three galaxies at $D \leq 10$ kpc, one is at low redshift where the angular separation from the quasar is much greater than the quasar seeing disk, and the other two were found at higher redshift following point spread function subtraction of the quasar (Steidel, Dickinson, & Persson 1994), which was not performed in all surveys.

within a fixed projected separation increases as the minimum absorption threshold is lowered. The covering fraction may exhibit a luminosity dependence for $W_{\text{cut}} = 0.1$ and 0.3 \AA such that low luminosity galaxies have larger covering fractions than high luminosity galaxies, but this is most apparent outside of $D = 100$ kpc where the covering fraction is less robust. We find no luminosity dependence for $W_{\text{cut}} = 0.6 \text{ \AA}$. For $W_{\text{cut}} = 1.0 \text{ \AA}$, $f_{D_{\text{max}}}$ is larger for high luminosity galaxies at all D_{max} than for low luminosity galaxies. This difference is accentuated at $D_{\text{max}} \leq 50$ kpc.

In the middle panels of Figure 3, we present $f_{D_{\text{max}}}$ and its uncertainties versus D_{max} for red and blue galaxies. The mean redshift for red galaxies is $\bar{z} = 0.36$ over the range $0.1 \leq z \leq 0.85$, and for blue galaxies $\bar{z} = 0.44$ over $0.1 \leq z \leq 1.02$. For the $W_{\text{cut}} = 0.1, 0.3,$ and 0.6 \AA subsamples, blue galaxies have higher covering fractions relative to red galaxies for $D_{\text{max}} > 50$ kpc. Within 50 kpc, the larger uncertainties make it difficult to distinguish any possible differences. For $W_{\text{cut}} = 1.0 \text{ \AA}$, the covering fractions for red and blue galaxies are indistinguishable outside of $D = 50$ kpc. Within $D = 50$ kpc, red galaxies may have larger covering fractions, though the un-

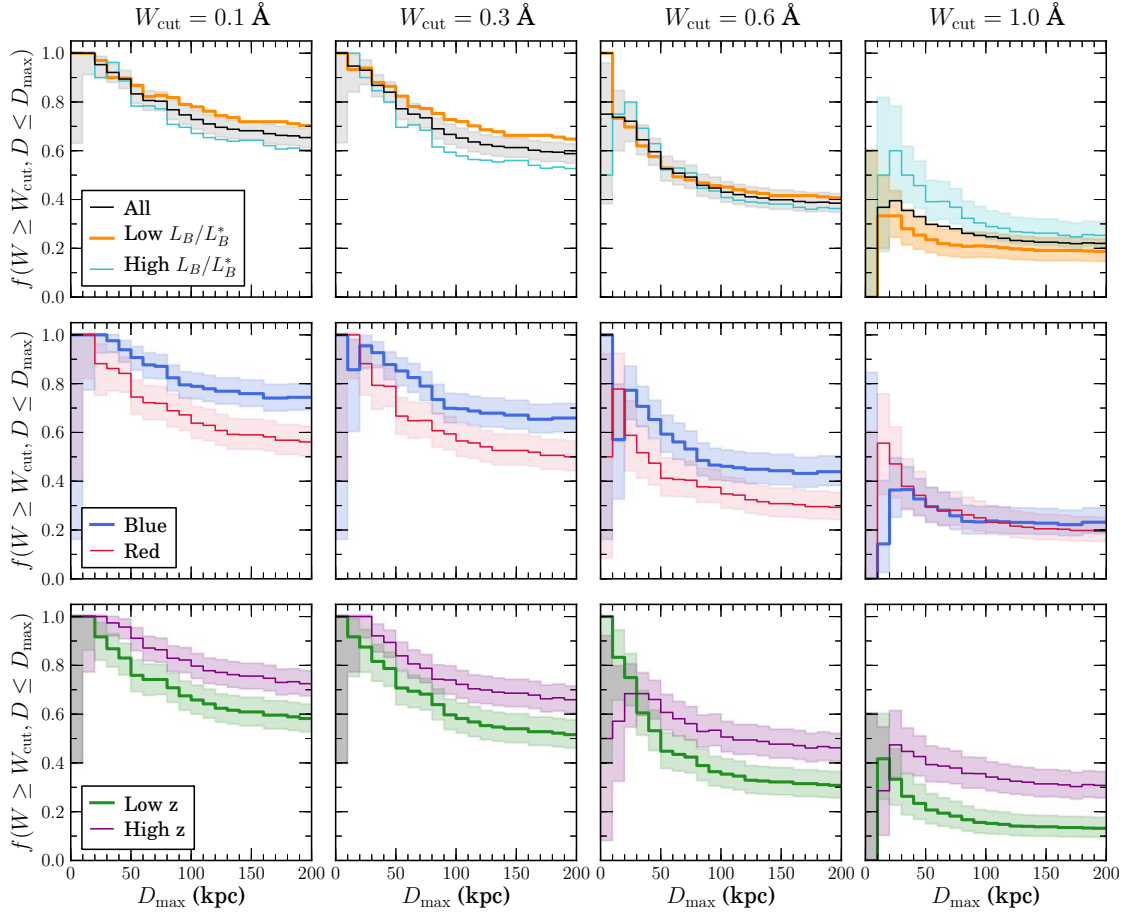


FIG. 3.— The covering fraction, $f_{D_{\max}}$, inside D_{\max} for different bifurcated subsamples split at the median L_B/L_B^* , $B-K$, and z_{gal} and for various $W_r(2796) > W_{\text{cut}}$ thresholds. Shaded regions represent 1σ uncertainties based upon binomial statistics. — (upper) The full sample of galaxies (thin black line), the high luminosity galaxies (thin blue line), and the low luminosity galaxies (thick orange line), divided at the median B -band luminosity, $L_B/L_B^* = 0.611$. — (middle) The blue ($B-K < 1.48$) and red ($B-K > 1.48$) galaxy subsamples bifurcated at the median galaxy color. — (lower) The high ($z \geq \langle z \rangle$) and low ($z < \langle z \rangle$) redshift galaxy subsamples where $\langle z \rangle = 0.359$.

certainties are again large.

In Figure 3 (lower panels), we present $f_{D_{\max}}$ and its uncertainties against D_{\max} for the high z and low z galaxy subsamples. For $D_{\max} \leq 50$ kpc, it is difficult to distinguish any redshift evolution in $f_{D_{\max}}$ due to the uncertainties. Beyond 50 kpc, the data suggest that $f_{D_{\max}}$ may evolve such that at higher redshift, the covering fraction of MgII absorbing gas is higher than at lower redshift.

Chen et al. (2010a) also examined the luminosity dependence of $f_{D_{\max}}$ as a function of W_{cut} , where their D_{\max} is fixed at the luminosity scaled “gas radius”, with $R_{\text{gas}} \propto (L_B/L_B^*)^{0.35}$, assuming isothermal density profile (Tinker & Chen 2008) and NFW profile (Navarro et al. 1996) models. As such, a direct comparison with our non-parameterized results is difficult. Nonetheless, they found that $f_{D_{\max}}$ has little to no dependence on galaxy B -band luminosity for $W_{\text{cut}} = 0.1, 0.3$, and 0.5 \AA , which is consistent with our result; however, for $W_{\text{cut}} = 1.0 \text{ \AA}$, we found systematically larger $f_{D_{\max}}$ for high luminosity galaxies as compared to low luminosity galaxies, especially for $D_{\max} \leq 50$ kpc.

3.4.2. Covering Fraction Profiles

To examine the covering fraction profile with projected distance from the galaxy, we computed $f_{\langle D \rangle} \equiv f(W \geq W_{\text{cut}}, \langle D \rangle)$, which we define as the fraction of absorbers with $W_r(2796) \geq W_{\text{cut}}$ in fixed impact parameter bins. We select the bins

$0 \leq D < 25$ kpc, $25 \leq D < 50$ kpc, $50 \leq D < 100$ kpc, and $100 \leq D < 200$ kpc, for which $\langle D \rangle$ is the average impact parameter of the galaxies in the bin.

In Figure 4, we plot $f_{\langle D \rangle}$ against $\langle D \rangle$. The horizontal bars are the impact parameter ranges and the data points are the average impact parameters, $\langle D \rangle$, for each bin. The vertical error bars are the 1σ uncertainties in $f_{\langle D \rangle}$ based upon binomial statistics. The subsamples presented in each panel are identical to the corresponding panels of Figure 3.

As can be seen in the upper panels of Figure 4, the $f_{\langle D \rangle}$ profile decreases as impact parameter is increased and this behavior is exhibited regardless of W_{cut} . Also note that as W_{cut} is increased, $f_{\langle D \rangle}$ is smaller for a given impact parameter bin. This indicates that in a fixed annulus around galaxies, the sky-projected distribution of the MgII CGM becomes progressively patchier as higher column density material and/or more complex kinematics are selected. For $W_{\text{cut}} = 0.1 \text{ \AA}$, the $f_{\langle D \rangle}$ profile decreases from unity within a radius of 25 kpc to 30% in the annulus 100–200 kpc, whereas for $W_{\text{cut}} = 1.0 \text{ \AA}$, the covering fraction decreases from 40% to less than 10%.

Also shown in the upper panels of Figure 4 is $f_{\langle D \rangle}$ split by $L_B/L_B^* = 0.611$. For low luminosity galaxies, the covering fraction vanishes outside of $D = 100$ kpc for all W_{cut} . On the other hand, in the annulus 100–200 kpc, the covering fractions for high luminosity galaxies are approximately 50%, 40%, 15%, and 10% for $W_{\text{cut}} = 0.1, 0.3, 0.6$, and 1.0 \AA , respectively.

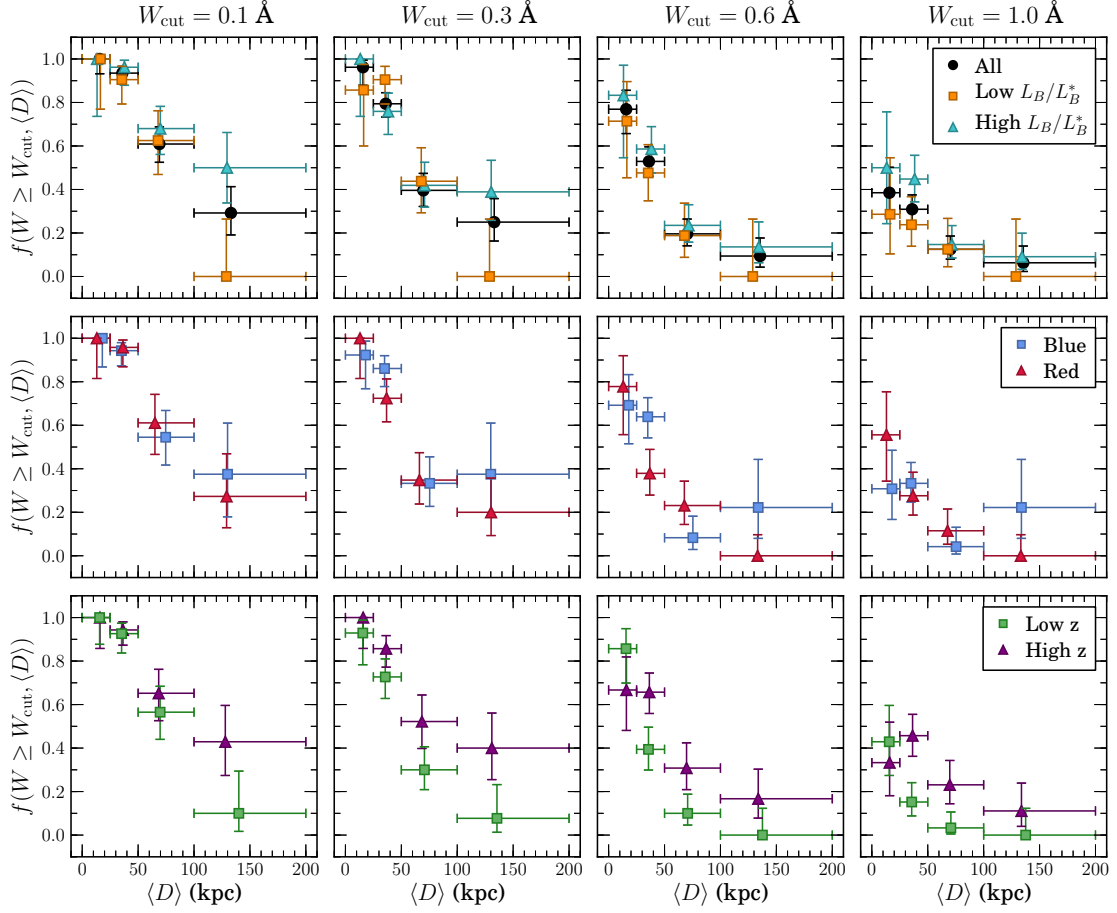


FIG. 4.— The covering fraction profile, $f_{(D)}$, for the impact parameter bins $0 \leq D < 25$ kpc, $25 \leq D < 50$ kpc, $50 \leq D < 100$ kpc, and $100 \leq D < 200$ kpc for different $W_r(2796)$ thresholds, W_{cut} . The horizontal bars indicate the impact parameter bin width and the vertical bars are the 1σ binomial uncertainties. Data points are plotted at the mean impact parameter of the galaxies in the bin. — (upper) The full sample of galaxies (solid black circles), the high luminosity galaxies (blue triangles), and the low luminosity galaxies (orange squares). — (middle) Blue (blue squares) and red (red triangles) galaxy subsamples sliced at the median galaxy color. — (lower) High (purple triangles) and low (green squares) redshift subsamples cut by the median redshift, $\langle z \rangle = 0.359$.

TABLE 2
LUMINOSITY DEPENDENCE OF COVERING FRACTION PROFILES, $f_{(D)}$

$W_{\text{cut}}, \text{\AA}$	(0–25), kpc	[25–50), kpc	[50–100), kpc	[100–200), kpc
All Galaxies				
0.1	$1.00^{+0.00}_{-0.07}$	$0.94^{+0.03}_{-0.05}$	$0.61^{+0.08}_{-0.08}$	$0.29^{+0.12}_{-0.10}$
0.3	$0.96^{+0.03}_{-0.08}$	$0.79^{+0.05}_{-0.06}$	$0.40^{+0.08}_{-0.07}$	$0.25^{+0.11}_{-0.09}$
0.6	$0.77^{+0.09}_{-0.11}$	$0.53^{+0.07}_{-0.07}$	$0.20^{+0.07}_{-0.06}$	$0.09^{+0.08}_{-0.05}$
1.0	$0.39^{+0.12}_{-0.11}$	$0.31^{+0.07}_{-0.06}$	$0.13^{+0.06}_{-0.05}$	$0.06^{+0.08}_{-0.04}$
Low L_B/L_B^* Galaxies				
0.1	$1.00^{+0.00}_{-0.23}$	$0.91^{+0.06}_{-0.11}$	$0.63^{+0.14}_{-0.16}$	$0.00^{+0.26}_{-0.00}$
0.3	$0.86^{+0.12}_{-0.26}$	$0.91^{+0.06}_{-0.11}$	$0.44^{+0.15}_{-0.15}$	$0.00^{+0.26}_{-0.00}$
0.6	$0.71^{+0.18}_{-0.26}$	$0.48^{+0.13}_{-0.13}$	$0.19^{+0.15}_{-0.10}$	$0.00^{+0.26}_{-0.00}$
1.0	$0.29^{+0.26}_{-0.18}$	$0.24^{+0.13}_{-0.10}$	$0.13^{+0.14}_{-0.08}$	$0.00^{+0.26}_{-0.00}$
High L_B/L_B^* Galaxies				
0.1	$1.00^{+0.00}_{-0.26}$	$0.96^{+0.03}_{-0.08}$	$0.68^{+0.10}_{-0.12}$	$0.50^{+0.16}_{-0.16}$
0.3	$1.00^{+0.00}_{-0.26}$	$0.76^{+0.08}_{-0.10}$	$0.42^{+0.11}_{-0.10}$	$0.39^{+0.15}_{-0.13}$
0.6	$0.83^{+0.14}_{-0.29}$	$0.59^{+0.10}_{-0.11}$	$0.24^{+0.10}_{-0.08}$	$0.14^{+0.12}_{-0.07}$
1.0	$0.50^{+0.26}_{-0.26}$	$0.45^{+0.11}_{-0.11}$	$0.15^{+0.09}_{-0.06}$	$0.09^{+0.11}_{-0.06}$

Covering fraction profiles for all, low, and, high luminosity galaxies are listed in Table 2.

The data are suggestive of a luminosity dependence for the maximum extent of MgII absorbing gas, such that the CGM of low L_B/L_B^* galaxies extends no further than 100 kpc, whereas high luminosity galaxies have a detectable MgII CGM beyond 100 kpc. The difference between high and low luminosity galaxies is most prominent outside of 100 kpc for $W_{\text{cut}} = 0.1$, and 0.3 \AA . As such, high luminosity galaxies exhibit a more extended MgII CGM, whereas for low luminosity galaxies, the MgII CGM is more concentrated in the central regions but with relatively lower covering fraction as W_{cut} is increased.

In the middle panels of Figure 4, the covering fraction profiles of red and blue galaxies exhibit several differences. Note that for red galaxies, none have absorption with $W_r(2796) \geq 0.6 \text{ \AA}$ in the range 100–200 kpc. Blue galaxies consistently have covering fractions of approximately 40% for $W_{\text{cut}} \leq 0.3 \text{ \AA}$ and 20% for $W_r(2796) \geq 0.6 \text{ \AA}$ in the range 100–200 kpc. Within 25 kpc the covering fraction for blue galaxies drops more rapidly than for red galaxies with increasing W_{cut} . Moreover, for $W_{\text{cut}} = 0.6$ and 1.0 \AA there is a hint that the covering fraction of red galaxies drops more rapidly for $D > 25$ kpc relative to the $D = 0$ –25 kpc region. This may suggest that the gas in red galaxies is more concentrated near the center while in blue galaxies, the gas is not as highly concentrated.

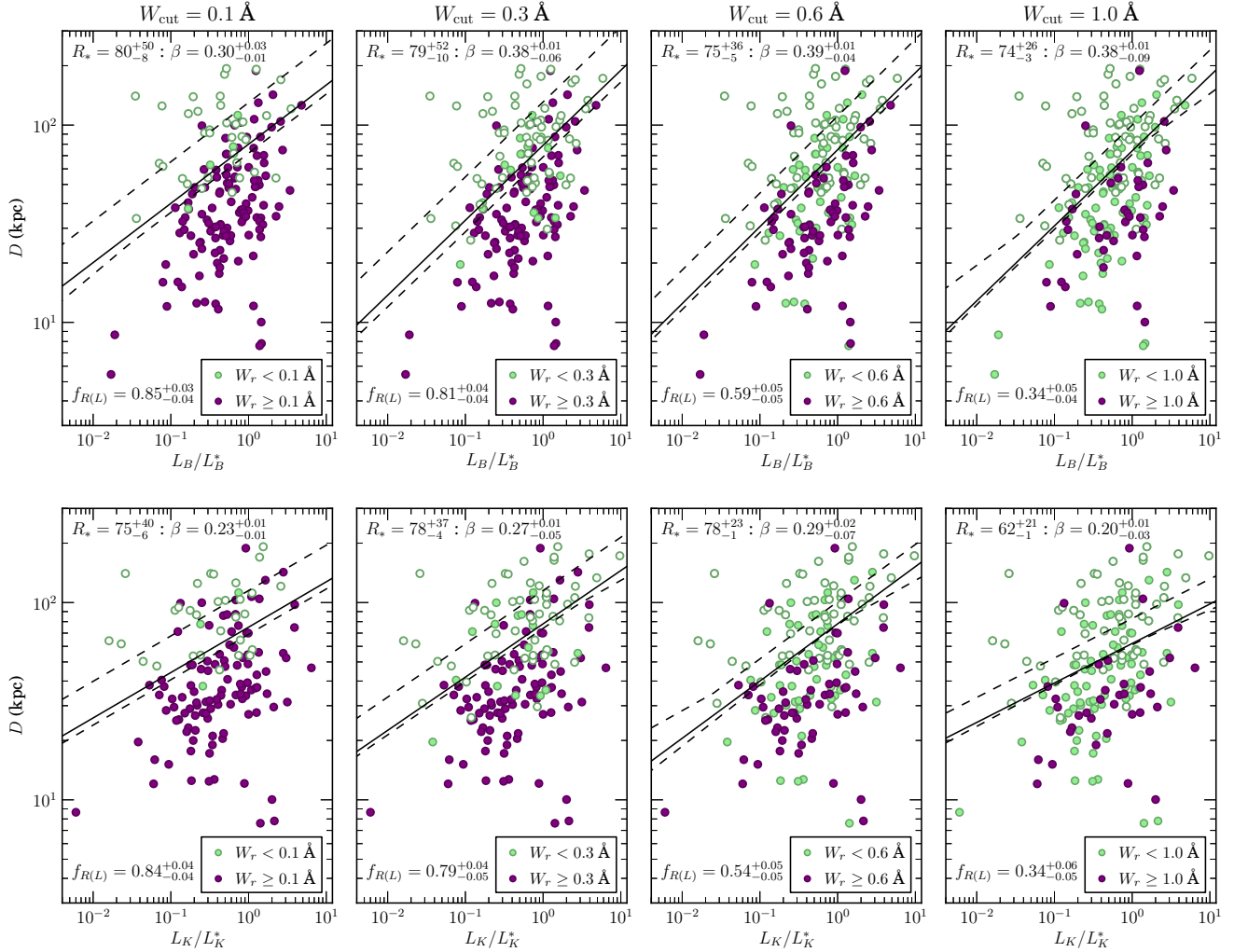


FIG. 5.— Impact parameter, D , versus luminosity for different $W_r(2796)$ bifurcations at W_{cut} . Green points are galaxies with $W_r(2796) < W_{\text{cut}}$ (solid points) or an upper limit on absorption (open points) and purple points are galaxies with $W_r(2796) \geq W_{\text{cut}}$. — (upper) B -band luminosity. — (lower) K -band luminosity. The fit parameters R_* , β , and $f_{R(L)}$ give the absorbing gas halo radius for an L^* galaxy, luminosity scaling power index, and absorption covering fraction, respectively, for each $W_r(2796) = W_{\text{cut}}$ threshold (see Table 3). Dashed lines provide the envelope 1σ uncertainties in the fit at fixed L/L^* . For $W_{\text{cut}} = 0.1 \text{ \AA}$, galaxies with an upper limit on absorption greater than 0.1 \AA were not included in the fitting process and are therefore not plotted.

As shown in the lower panels of Figure 4, high redshift galaxies exhibit a trend of higher $f_{(D)}$ in the 25–50, 50–100, and 100–200 kpc annuli relative to low redshift galaxies. Within 25 kpc, the covering fraction may be higher in low redshift galaxies for stronger absorption, $W_{\text{cut}} = 0.6$ and 1.0 \AA . Though the trends are marginal, they may suggest a greater extension of the gas at higher redshift followed by a settling of material into the inner regions at lower redshift.

Chen et al. (2010a) examined $f_{(D)}$ for their sample ($\langle z \rangle = 0.25$), and also found that the covering fraction profile, $f_{(D)}$, decreases with increasing D and is smaller at a given $\langle D \rangle$ with increasing W_{cut} using $W_{\text{cut}} = 0.1, 0.3$, and 0.5 \AA . However, a direct comparison with our results is difficult because Chen et al. (2010a) scale D assuming a B -band galaxy luminosity dependent “gas radius” proportional to $(L_B/L_B^*)^{0.35}$.

3.5. Luminosity Scaling and Covering Fraction

Our results in the previous section strongly suggest that the MgII absorbing CGM extends further for weaker absorption than for stronger absorption, and that this behavior has a clear dependence with galaxy luminosity. What is further clear, is that for a given W_{cut} , the CGM becomes more “patchy”

TABLE 3
LUMINOSITY SCALED HALO ABSORPTION RADII

W_{cut} [Å]	B-band			K-band		
	R_* [kpc]	β	$f_{R(L)}$	R_* [kpc]	β	$f_{R(L)}$
0.1	80^{+50}_{-8}	$0.30^{+0.03}_{-0.01}$	$0.85^{+0.03}_{-0.04}$	75^{+40}_{-6}	$0.23^{+0.01}_{-0.01}$	$0.84^{+0.04}_{-0.04}$
0.3	79^{+52}_{-10}	$0.38^{+0.01}_{-0.06}$	$0.81^{+0.04}_{-0.04}$	78^{+37}_{-4}	$0.27^{+0.01}_{-0.05}$	$0.79^{+0.04}_{-0.05}$
0.6	75^{+36}_{-5}	$0.39^{+0.01}_{-0.04}$	$0.59^{+0.05}_{-0.05}$	78^{+23}_{-1}	$0.29^{+0.02}_{-0.07}$	$0.54^{+0.05}_{-0.05}$
1.0	74^{+26}_{-3}	$0.38^{+0.01}_{-0.09}$	$0.34^{+0.05}_{-0.04}$	62^{+21}_{-1}	$0.20^{+0.01}_{-0.03}$	$0.34^{+0.06}_{-0.05}$

with increasing D , as indicated by the decreasing covering fractions. As such, it would seem that the notion of a well-defined MgII CGM “gas radius”, or “halo absorption radius” is an oversimplification in that the extent of the gas exhibits a “fuzzy” boundary when averaged over many galaxies. Nonetheless, for historical comparisons we parameterize the characteristics of an “outer” boundary and its plausible dependence on the galaxy properties and redshift.

Since the work of Bergeron & Boissè (1991), the extent of absorbing gas is commonly assumed to follow a Holmberg-

like relation, $R(L) = R_*(L/L^*)^\beta$. We examined whether the halo absorption radius also depends on $W_r(2796)$, and/or galaxy color and redshift.

To examine the dependence on $W_r(2796)$, we adopt $W_{\text{cut}} = 0.1, 0.3, 0.6,$ and 1.0 \AA . To estimate R_* and β , we varied the two parameters over the ranges $0 \leq R_* \leq 300 \text{ kpc}$ and $0 \leq \beta \leq 1$ and computed the function $q(R_*, \beta, L, W_{\text{cut}}) = wr_{(\geq)} + r_{(<)}$, where $r_{(\geq)}$ is the fraction of systems with $W_r(2796) \geq W_{\text{cut}}$ below $R(L)$, $r_{(<)}$ is the fraction with $W_r(2796) < W_{\text{cut}}$ above $R(L)$, and w is a weighting factor⁵. The parameter values are adopted when $q(R_*, \beta, L, W_{\text{cut}})$ is a maximum, for which the covering fraction inside $R(L)$ is $f_{R(L)} = 1/(1+x)$, where $x = (n_{(\geq)}/n_{(<)}) (1 - r_{(<)}) / r_{(\geq)}$, and where $n_{(\geq)}$ and $n_{(<)}$ are the number of systems with $W_r(2796) \geq W_{\text{cut}}$ and $W_r(2796) < W_{\text{cut}}$, respectively.

The downward and upward 1σ uncertainties in R_* were estimated by using the best estimate of β and performing one-sided integration under the $q(R_*, \beta, L, W_{\text{cut}})$ curve until 84.13% of the total area was obtained. Similarly, the downward and upward 1σ uncertainties in β were estimated by using the best estimate of R_* . The 1σ uncertainties in $f_{R(L)}$ are computed using binomial statistics by computing the fraction of galaxies with $W_r(2796) \geq W_{\text{cut}}$ to all galaxies within $R(L)$.

Our results are presented in Table 3 for both B - and K -band luminosities. In the upper panels of Figure 5, we present D against L_B/L_B^* . The luminosity scaling increases from $\beta \sim 0.3$ for $W_{\text{cut}} = 0.1 \text{ \AA}$ to $\beta \sim 0.4$ for $W_{\text{cut}} = 0.3, 0.6,$ and 1.0 \AA . The absorbing gas halo radius, R_* , for an L_B^* galaxy is on the order of $\sim 80 \text{ kpc}$ for $W_{\text{cut}} = 0.1$ and 0.3 \AA , while R_* is on the order of $\sim 75 \text{ kpc}$ (but consistent with 80 kpc , given the uncertainties in R_*) for $W_{\text{cut}} = 0.6$ and 1.0 \AA . The covering fraction decreases from $f_{R(L)} = 0.85$ for $W_{\text{cut}} = 0.1 \text{ \AA}$ to 0.34 for $W_{\text{cut}} = 1.0 \text{ \AA}$.

In the lower panels of Figure 5, we present the K -band results. We note that this subsample has 18 fewer galaxies than the B -band subsample. The luminosity scaling varies from ~ 0.2 for $W_{\text{cut}} = 0.1$ and 1.0 \AA to ~ 0.3 for $W_{\text{cut}} = 0.3$ and 0.6 \AA . The halo absorption radius also has a range of values where $R_* = 75 \text{ kpc}$ for $W_{\text{cut}} = 0.1 \text{ \AA}$, 78 kpc for 0.3 and 0.6 \AA , and 62 kpc for 1.0 \AA , however, these values are all consistent within uncertainties. The covering fraction behaves similarly to the B -band (see Table 3).

Steidel (1995) reported $\beta \simeq 0.2$ and $R_* = 55 \text{ kpc}$ for the B -band and $\beta \simeq 0.15$ and $R_* = 58 \text{ kpc}$ for the K -band, both for $W_{\text{cut}} = 0.3 \text{ \AA}$ (the values of R_* quoted here have been converted to a “737” Λ CDM cosmology at the mean redshift, $\langle z \rangle = 0.65$, of his sample). He deduced a covering fraction of $f_{R(L)} \simeq 1$ and that β and R_* for the K -band are slightly smaller than for the B -band. Guillemin & Bergeron (1997) obtained similar results, with $R_* = 47 \text{ kpc}$ (adjusted from $q_0 = 0.05$ and h_{50} at $z = 0.7$) and $\beta = 0.28$ for the B -band with $W_{\text{cut}} \simeq 0.3 \text{ \AA}$.

Using the observed MgII absorber redshift path number density as a constraint, Kacprzak et al. (2008) explored the parameter space of the minimum luminosity of MgII absorption-selected galaxies; the slope, β ; the halo absorption radius, R_* ; and covering fraction, $f_{R(L)}$. For $W_{\text{cut}} = 0.3 \text{ \AA}$, they constrained R_* to the range 50 – 110 kpc , β to the range 0.2 – 0.28 , and $f_{R(L)}$ to the range 50 – 80% . Our values of R_*

⁵ Since we wish to determine the “outer envelope” of the halo absorption radius, we adopt the weight $w = 2$. When $w = 1$, we find β consistent with zero.

reside in the range of allowed values from their study.

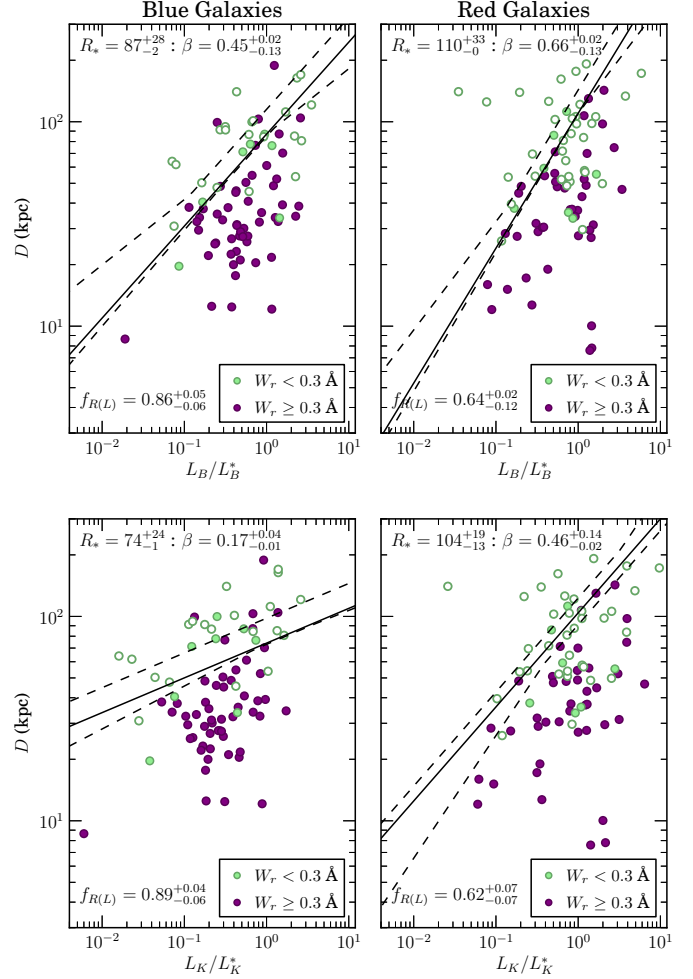


FIG. 6.— Impact parameter, D , versus L_B/L_B^* (top) and L_K/L_K^* (bottom) for blue and red galaxies split by the median color $B-K = 1.48$. Point types and curves are the same as Figure 5 for $W_{\text{cut}} = 0.3 \text{ \AA}$. The luminosity scaling, β , and radius, R_* , of the absorbing gas halo radius exhibits a color dependence for this W_{cut} . In the B -band, blue galaxies have a steeper luminosity scaling, larger R_* , and larger covering fraction than red galaxies. For the K -band, we find R_* and β to be larger in red galaxies than blue, while blue galaxies still have a larger covering fraction.

Chen et al. (2010a) reported $R_* = 107 \text{ kpc}$ with $\beta = 0.35$ for the B -band, where they fitted their data in the context of an isothermal sphere model (see Tinker & Chen 2008) of the MgII CGM. For these values, they find $f_{R(L)} = 0.7$ for $W_{\text{cut}} = 0.3 \text{ \AA}$ and $f_{R(L)} = 0.8$ for $W_{\text{cut}} = 0.1 \text{ \AA}$, both of which are $\sim 10\%$ smaller than what we find.

Employing the Tinker & Chen (2008) isothermal sphere model, Bordoloi et al. (2011) deduced $R_* = 115 \text{ kpc}$. Whereas β for this work is consistent with the value reported by Chen et al. (2010a), the larger values of R_* reported by both Chen et al. (2010a) and Bordoloi et al. (2011) may be an artifact of their application of a model to the data. Furthermore, the methods of Bordoloi et al. (2011) involve “averaging” over annuli of fixed impact parameter, which may introduce an additional systematic.

3.5.1. Galaxy Color

To examine the dependence of $R(L)$ on galaxy color, we computed R_* , β , and $f_{R(L)}$ for red and blue galaxies, bifur-

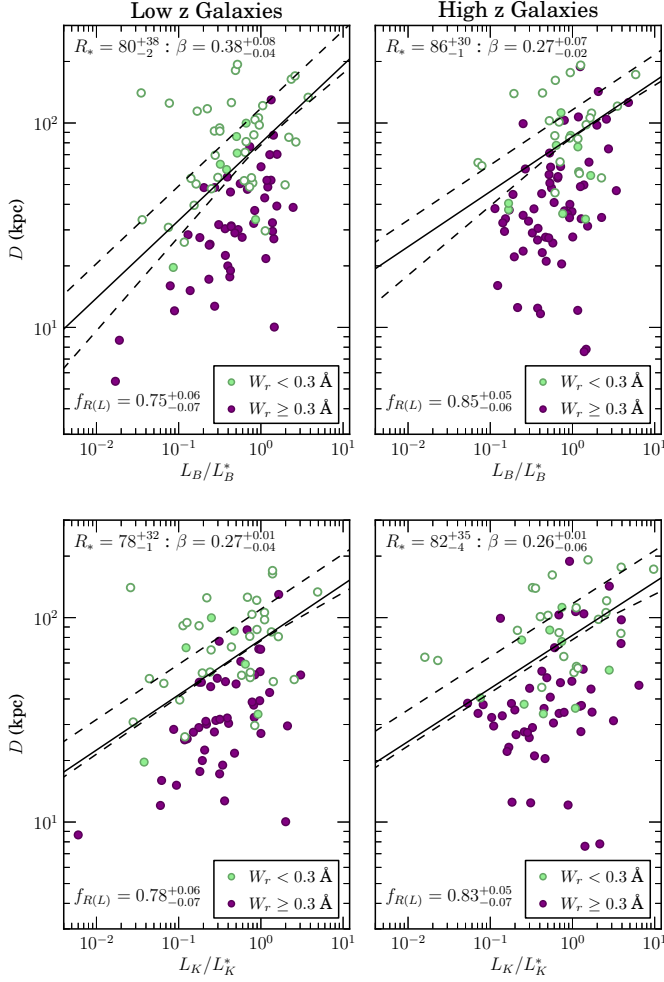


FIG. 7.— Impact parameter, D , versus L_B/L_B^* (top) and L_K/L_K^* (bottom) for low and high redshift galaxies sliced by the median redshift $z_{\text{gal}} = 0.359$. Point types and curves are the same as Figure 5 for $W_{\text{cut}} = 0.3 \text{ \AA}$. The average z for the low redshift subsample is 0.23 and the average for the high redshift subsample is 0.61, which is a ~ 3.2 Gyr difference.

cated by $B-K = 1.48$, in both the B - and K -bands. Due to the smaller number of galaxies in the blue and red subsamples (82 each), we adopted a single equivalent width cut, $W_{\text{cut}} = 0.3 \text{ \AA}$ (the median $W_r(2796)$ for galaxies with measured colors). As shown in Figure 6 and tabulated in Table 4, the parameters for $R(L)$ suggest a dependence on galaxy color in both the B - and K -bands.

In the B -band (top panels of Figure 6), we find that red galaxies have a steeper luminosity scaling, $\beta \sim 0.7$, than blue galaxies, $\beta \sim 0.5$, but a smaller covering fraction, $f_{R(L)} = 0.6$, than blue galaxies, $f_{R(L)} = 0.9$. The halo absorption radius for red galaxies, $R_* \sim 110$ kpc, is larger than for blue galaxies, $R_* \sim 87$ kpc. However, both values of R_* are consistent within uncertainties. These values are smaller than the model dependent values found by Bordoloi et al. (2011), who report 118 kpc for red galaxies and 107 kpc for blue galaxies, but the behavior of R_* with color is similar in that our red galaxies have larger R_* than blue galaxies.

The $R(L)$ dependence on galaxy color is similar in the K -band (bottom panels of Figure 6). The halo absorption radius, R_* , is again larger for red galaxies (though the values are still consistent within uncertainties), with $R_* \sim 75$ kpc and $R_* \sim 105$ kpc for blue and red galaxies, respectively. The luminosity scaling is steeper in red galaxies, $\beta \sim 0.5$, than blue

TABLE 4
LUMINOSITY SCALING FOR SUBSAMPLES AT $W_{\text{cut}} = 0.3 \text{ \AA}$

Sample	B-band			K-band		
	R_* [kpc]	β	$f_{R(L)}$	R_* [kpc]	β	$f_{R(L)}$
All	80^{+50}_{-8}	$0.30^{+0.03}_{-0.01}$	$0.85^{+0.03}_{-0.04}$	75^{+40}_{-6}	$0.23^{+0.01}_{-0.01}$	$0.84^{+0.04}_{-0.04}$
Blue	87^{+28}_{-2}	$0.45^{+0.02}_{-0.13}$	$0.86^{+0.05}_{-0.06}$	74^{+24}_{-1}	$0.17^{+0.04}_{-0.01}$	$0.89^{+0.04}_{-0.06}$
Red	110^{+33}_{-0}	$0.66^{+0.02}_{-0.13}$	$0.64^{+0.02}_{-0.12}$	104^{+19}_{-13}	$0.46^{+0.14}_{-0.02}$	$0.62^{+0.07}_{-0.07}$
Low z	$80^{+38}_{-0.4}$	$0.38^{+0.08}_{-0.04}$	$0.75^{+0.06}_{-0.07}$	78^{+32}_{-1}	$0.27^{+0.01}_{-0.04}$	$0.78^{+0.06}_{-0.07}$
High z	86^{+30}_{-1}	$0.27^{+0.07}_{-0.02}$	$0.85^{+0.05}_{-0.06}$	82^{+35}_{-4}	$0.26^{+0.01}_{-0.06}$	$0.83^{+0.05}_{-0.07}$

galaxies, $\beta \sim 0.2$, and the covering fraction is larger in blue galaxies than red galaxies ($f_{R(L)} \sim 0.9$ and $f_{R(L)} \sim 0.6$, respectively).

3.5.2. Galaxy Redshift

We also examined the $R(L)$ dependence in both the B - and K -bands on galaxy redshift, slicing the sample into low and high redshift galaxies by the median redshift (z) = 0.359, and adopting $W_{\text{cut}} = 0.3 \text{ \AA}$. Values for R_* , β , and $f_{R(L)}$ are presented in Figure 7 and tabulated in Table 4.

In the B -band (top panels of Figure 7), we find $R_* \sim 80$ kpc, $\beta \sim 0.4$, and $f_{R(L)} \sim 0.75$ in the low z subsample. The high z subsample has similar values for R_* (~ 85 kpc) and $f_{R(L)}$ (~ 0.8), but a much shallower dependence on L_B/L_B^* , with $\beta \sim 0.3$. This difference in β may be due to selection effects in that the lowest luminosity galaxies ($L_B/L_B^* < 0.1$) are being selected against at high redshift. The selection methods for MAGICAT galaxies are detailed in Paper I (Nielsen et al. 2013). Additionally, the presence of galaxies at low z and low impact parameter may bias β to a larger value.

On the other hand, the K -band (bottom panels of Figure 7) shows no discernable difference within uncertainties between the low and high z subsamples. The values for R_* , β , and $f_{R(L)}$ for both subsamples are ~ 80 kpc, ~ 0.3 , and ~ 0.8 , respectively. Comparing to the apparent B -band evolution, this may imply that the luminosity dependence of the extent of the Mg II absorbing CGM is unchanged with redshift for the K -band. An alternate explanation is that the K -band is not impacted by selection effects as much as the B -band since K -band absolute magnitudes and luminosities were calculated from apparent K -band magnitudes for half of the sample. The K -band apparent magnitude is not one of the galaxy selection criteria (Nielsen et al. 2013).

4. DISCUSSION

With the larger sample afforded by MAGICAT, we have obtained additional leverage to probe the dependence of the properties of the Mg II absorbing CGM with galaxy color, redshift, luminosity, impact parameter, and $W_r(2796)$ threshold. For our analysis, we have purposely avoided couching the data within the framework of model expectations or scaling various measured quantities with “second parameters”, such as scaling the impact parameter by galaxy luminosity, in order to provide a direct view of the CGM-galaxy connection and to interpret the data from a purely observational perspective.

We confirm the well-known anti-correlation between Mg II equivalent width, $W_r(2796)$, and impact parameter, D , which is significant to the 7.9σ level. We find that the general behavior of this anti-correlation on the $W_r(2796)$ – D plane is

best fit by a log-linear fit to the data, $\log W_r(2796) = \alpha_1 D + \alpha_2$, where $\alpha_1 = -0.015 \pm 0.002$ and $\alpha_2 = 0.27 \pm 0.11$. This is in contrast to the power law fit obtained by Chen et al. (2010a). Our log-linear fit predicts a leveling off of $W_r(2796)$ as D goes to zero, whereas the Chen et al. (2010a) fit does not. In fact, for $D = 5$ kpc, which is roughly the smallest impact parameter in MAGIIICAT, our log-linear fit predicts $W_r(2796) \simeq 1.6 \text{ \AA}$, while the power law predicts $W_r(2796) \simeq 4.4 \text{ \AA}$ (and continues to increase, for example at $D = 1$ kpc, the power law fit predicts $W_r(2796) \simeq 30 \text{ \AA}$). It would seem reasonable that the equivalent width distribution should flatten as one probes galaxy disks as $W_r(2796) > 10 \text{ \AA}$ has yet to be reported in the literature, even for the Milky Way interstellar medium.

As many previous works have noted (see § 3.3 for references), there is considerable scatter in the $W_r(2796) - D$ plane, which we also observe in Figure 1. Slicing MAGIIICAT by the median values of $B - K$, z_{gal} , L_B/L_B^* , and L_K/L_K^* (see Figure 2), we find that the scatter is not related to galaxy color or redshift. However, we do find that the scatter may be related to galaxy luminosities such that higher luminosity galaxies systematically populate the $W_r(2796) - D$ plane at larger $W_r(2796)$ and larger D . Performing a 2DKS test on luminosities in the $W_r(2796) - D$ plane, we find this result to be significant to the 4.2σ level for the B -band and to the 4.3σ level for the K -band. Given that the K -band can be considered a proxy for stellar mass, this result may indicate that the scatter in the $W_r(2796) - D$ plane is actually due to galaxy mass such that more massive galaxies have larger $W_r(2796)$ for a given D . In fact, Churchill et al. (2013b) find this to be true for MAGIIICAT galaxies with the galaxy virial mass obtained using halo abundance matching.

Alternatively, the luminosity segregation on the $W_r(2796) - D$ plane may be due to a gas metallicity-luminosity correlation. For damped Ly α systems, Turnshek et al. (2005) found that gas metallicity correlates with Mg II equivalent width. If higher luminosity galaxies have more metal-rich gas, then $W_r(2796)$ would tend to be larger than for lower luminosity galaxies, and the gas would be detectable to larger impact parameters. This behavior on the $W_r(2796) - D$ plane might have some relationship to the observed metallicity bimodality in Lyman limit systems (Lehner et al. 2013).

With regard to the relationship between galaxy color and $W_r(2796)$, our results challenge those of previous studies. For the overall sample, we find no correlation between $W_r(2796)$ and $B - K$. However, we find that for the subsample with $W_r(2796) \geq 1 \text{ \AA}$, redder galaxies have larger $W_r(2796)$ with a significance level of 2.5σ . These findings are contrary to the results of Zibetti et al. (2007) and Bordoloi et al. (2011), who both report larger $W_r(2796)$ associated with bluer galaxies. It is difficult to rectify the inconsistencies of our findings with those works unless the solution originates in the different experimental methods.

Zibetti et al. (2007) developed an image stacking method in which the individual galaxies are not identified, but light from galaxies in various SDSS photometric bands are measured *relative to control fields* for which the quasars show no Mg II absorption. The color cuts of the galaxies studied by Bordoloi et al. (2011) are based upon a color-mass relation using $u - B$ colors. Furthermore, the equivalent widths measured by Bordoloi et al. (2011) are based on stacked spectra over fixed impact parameter annuli in which the Mg II doublet is not resolved, whereas those measured in this work are based upon pencil-beam probes of the CGM for which

all doublets are cleanly resolved. If the CGM is intrinsically patchy (see Churchill et al. 2013a) with covering fraction dependencies on $W_r(2796)$ threshold and galaxy luminosity (as we have demonstrated in this paper), then the two methods (statistical versus case-by-case) may be providing different but complimentary clues to the nature of the CGM.

Our analysis of the covering fraction profile of the Mg II absorbing CGM as a function of impact parameter, galaxy luminosity, and absorption strength threshold provides improved insights on the extent and distribution of the low ionization, metal-enriched CGM (see Figure 4 and Table 2). The decrease in the covering fraction with increasing absorption threshold indicates that the cross-section of the highest column density and/or most kinematically dispersed gas (plausibly winds material) is smaller than the cumulative cross-section including lower column density, kinematically quiescent gas (plausibly accretion material).

Additional insight is provided by the relative behavior of the covering fraction profile of low and high luminosity galaxies (bifurcated at $L_B/L_B^* = 0.611$). First, the Mg II absorbing CGM appears to extend no further than 100 kpc for low luminosity galaxies. Second, the CGM at $D \geq 100$ kpc surrounding high luminosity galaxies is dominated by lower column density, kinematically quiescent gas traced by $W_r(2796) < 0.6 \text{ \AA}$ absorption; the cross-section of this material increases as the equivalent width threshold is decreased to 0.1 \AA . In contrast, within $D < 100$ kpc, the observed frequencies of lower and higher column density CGM gas is not strongly dependent on galaxy luminosity for $W_{\text{cut}} = 0.1, 0.3, \text{ and } 0.6 \text{ \AA}$, but for $W_{\text{cut}} = 1.0 \text{ \AA}$, high luminosity galaxies have a higher observed frequency of Mg II absorbing CGM. For $D \leq 25$ kpc, the covering fraction is effectively unity for the thresholds $W_r(2796) \geq 0.1$ and 0.3 \AA , but declines for $W_r(2796) \geq 0.6$ and 1.0 \AA as the threshold is increased.

These results indicate a strong luminosity dependence in cross-sections and extent of the Mg II absorbing CGM such that high luminosity galaxies have both a much more extended diffuse CGM than low luminosity galaxies and higher filling factors of the highest column density material within 50 kpc as compared to low luminosity galaxies. Since the luminosity segregation we are employing is for the B -band, we could be seeing a connection between the CGM and young stars, such that the increased presence of young stars is related to a greater cross-section of higher column density gas in the inner regions of the galaxies and a more extended distribution of the lower column density gas in the outer regions of the galaxies (beyond 100 kpc). This would imply a stellar driven mechanism for distributing the gas further out into the CGM.

We also find a difference in the covering fraction as a function of galaxy color outside of 100 kpc. In this case, blue galaxies have higher covering fractions than red galaxies, which have no absorption beyond 100 kpc for the highest column density material ($W_r(2796) \geq 0.6 \text{ \AA}$). Blue galaxies are more likely to host the galactic-scale winds which lift more metal-rich material into the halo. Therefore, the larger covering fractions in blue galaxies could be due to more metal-rich material present at large impact parameters. Lehner et al. (2013) concluded that Lyman limit systems, which trace the cool CGM, have a bimodal metallicity distribution where the metal-poor branch is likely probing cold accretion streams while the metal-rich branch could be tracing recycled outflowing winds. Therefore, our implied stellar driven mechanism may be driving more metal-rich material into the CGM. This

metal-rich material may result in larger $W_r(2796)$, which in turn could cause higher covering fractions for more luminous galaxies at large impact parameters.

Following previous studies, we have assumed the relation $R(L) = R_*(L/L^*)^\beta$ to describe the “halo absorption radius” dependence on luminosity. For the B -band luminosity, we find that the sensitivity of $R(L)$ to luminosity (the parameter β , see Table 3 and Figure 5) increases as the equivalent width threshold is raised. For $W_r(2796) \geq 0.1 \text{ \AA}$, we find $\beta \simeq 0.3$, and for $W_r(2797) \geq 0.3, 0.6,$ and 1.0 \AA , we find $\beta \simeq 0.4$. The extent for an L_B^* galaxy decreases with increasing equivalent width threshold. We find $R_* \simeq 80 \text{ kpc}$ for $W_r(2796) \geq 0.1$ and 0.3 \AA , and $R_* \simeq 75 \text{ kpc}$ for $W_r(2796) \geq 0.6$ and 1.0 \AA , though these values are consistent within uncertainties. In the K -band, we find similar values of R_* ($\sim 80 \text{ kpc}$) for $W_{\text{cut}} = 0.1, 0.3,$ and 0.6 \AA , while the most optically thick gas has a much smaller absorption radius ($R_* \sim 60 \text{ kpc}$ for $W_{\text{cut}} = 1.0 \text{ \AA}$). Furthermore, we find a shallower dependence of $R(L)$ on the K -band luminosity, where β ranges from ~ 0.2 to ~ 0.3 . The greater extent in the most optically thick gas for the B -band compared to the K -band and the higher luminosity sensitivity to the B -band relative to the K -band would further strengthen the idea that the geometric extent and morphology of the MgII absorbing CGM is governed in large part by young stars.

There is an indication that galaxy color directly plays a role in governing the luminosity sensitivity of $R(L)$. For $W_r(2796) \geq 0.3 \text{ \AA}$, red galaxies have a remarkably steeper luminosity dependence than do blue galaxies in the B -band. For red galaxies, we find $\beta = 0.66$, whereas for blue galaxies, we find $\beta = 0.45$. In the B -band, the covering fraction within $R(L)$ of red galaxies is $\simeq 30\%$ lower than for blue galaxies. For the K -band, red galaxies still have a much steeper luminosity dependence ($\beta = 0.46$) than blue galaxies ($\beta = 0.17$), as well as a $\sim 40\%$ smaller covering fraction. In studying the K -band of Figure 6, it is apparent that red galaxies are, on average, brighter in the K -band than blue galaxies. Using the K -band luminosity as a proxy for stellar mass, this indicates that red galaxies are, on average, more massive than blue galaxies. Therefore, we may be seeing that the halo absorption radius depends on the mass of the galaxy such that more massive galaxies have larger halo absorption radii resulting in a larger β for redder, more massive galaxies. The dependence of the halo absorption radius on mass is explored in more depth in the third paper of this series (Churchill et al. 2013c).

We strongly caution that the function $R(L)$ should not be viewed as a well-defined outer boundary to the MgII absorbing CGM. The values of R_* and β are dependent on the sample and may change if we obtain more low luminosity galaxies with $L/L^* < 0.1$. We are confident, however, that larger luminosity galaxies have a more extended CGM, i.e., the value of β is positive for both the B - and K -bands. Additionally, examination of the data on the D - L/L^* plane shown in Figure 5 clearly reveals that a non-negligible number of galaxies with $W_r(2796)$ greater than the threshold cut also reside above the curve. The 1σ upper envelope of the $R(L)$ boundary characterizes the presence of these galaxies. These galaxies also drive the large upward uncertainties in the best fit R_* . Note that this uncertainty increases from $\simeq 26$ to $\simeq 50 \text{ kpc}$ as the absorption threshold is decreased from $W_r(2796) \geq 1.0$ to 0.1 \AA . This suggests that the $R(L)$ boundary is less well defined for the lower column density structures of the CGM. Physically, the behavior of the data in this regime of impact parameter and $W_r(2796)$ could either reflect a greater level of

patchiness in the low column density material residing in the outskirts of the CGM of individual galaxies or a broad range of CGM properties from galaxy to galaxy.

5. SUMMARY

Combining our previous studies and the extant works in the literature, we have compiled a “MgII Absorber-Galaxy Catalog” (MAGIICAT) of intermediate redshift galaxies and their associated circumgalactic medium (CGM) as probed using MgII $\lambda\lambda 2796, 2803$ absorption. Details of the MAGIICAT data are presented in Paper I (Nielsen et al. 2013). In this paper, we present results from a first analysis in which we compare only direct observables and avoid converting or scaling the data to a preferred CGM model, focusing exclusively on “isolated” galaxies, which are defined to have no neighboring galaxy within a projected distance of 100 kpc and line of sight velocity within 500 km s^{-1} .

The sample presented here comprises 182 galaxies toward 134 quasar sightlines over the redshift range $0.072 \leq z_{\text{gal}} \leq 1.120$, with median $\langle z \rangle = 0.359$. The rest-frame magnitudes range from $-16.1 \geq M_B \geq -23.1$ ($0.02 \leq L_B/L_B^* \leq 5.87$) and $-17.0 \geq M_K \geq -25.3$ ($0.006 \leq L_K/L_K^* \leq 9.71$) with AB rest-frame colors $0.04 \leq B-K \leq 4.09$. The median B -band luminosity is $L_B/L_B^* = 0.611$ and the median color is $B-K = 1.48$.

The main results are:

1. The mean M_B increases with increasing redshift (4.4σ), whereas M_K exhibits a weak trend to increase with redshift (2.2σ). Galaxy luminosities L_B/L_B^* and L_K/L_K^* do not evolve with redshift. The rest-frame $B-K$ color shows no redshift evolution, consistent with the findings of Zibetti et al. (2007).

2. There is no correlation between $W_r(2796)$ and $B-K$ for the full sample (1.3σ). However, for galaxies associated with $W_r(2796) \geq 1.0 \text{ \AA}$ absorption, $B-K$ correlates with $W_r(2796)$ at 2.5σ , indicating a trend that redder galaxies have stronger absorption in this equivalent width regime. In our sample, the distributions of $W_r(2796)$ within $D = 50 \text{ kpc}$ of blue ($B-K < 1.48$) and red ($B-K \geq 1.48$) galaxies are consistent with being drawn from the same parent distribution (0.3σ). The $W_r(2796)$ -color correlation in our sample conflicts with the $W_r(2796)$ -color anti-correlation reported by Zibetti et al. (2007). Both the $W_r(2796)$ -color correlation and the indistinguishable $W_r(2796)$ distributions in our sample are in conflict with the findings of Bordoloi et al. (2011), who report eight times stronger $W_r(2796)$ within $D = 50 \text{ kpc}$ associated with bluer galaxies.

3. Including upper limits on $W_r(2796)$, we find that the significance level of the well-known anti-correlation between $W_r(2796)$ and impact parameter, D , is 7.9σ for this sample. The best parameterization is a log-linear relation, for which we find $\log W_r(2796) = (-0.015 \pm 0.002)D + (0.27 \pm 0.11)$. The scatter in this relation may be due to the redshifts, colors, or luminosities of the galaxies. Splitting the sample by the K -band luminosity yields a 4.3σ significance that low and high L_K/L_K^* galaxies are separate populations on the $W_r(2796) - D$ plane such that higher K -band luminosity galaxies tend to have higher $W_r(2796)$ at a given impact parameter. Dividing the sample into quartiles based on the redshift, color, or luminosity of the galaxies and comparing the lowest and highest quartiles yields at best a 3.4σ significance with K -band luminosity.

4. The covering fraction profiles with projected distance from the galaxy, $f_{D_{\text{max}}}$ and $f_{(D)}$, decrease with both increasing D and increasing minimum $W_r(2796)$ (see Figures 3 and 4). High luminosity galaxies have higher covering fractions. In

terms of $f_{(D)}$, this difference is greatest at $100 < D \leq 200$ kpc for absorbing CGM gas with $W_r(2796) \geq 0.1 \text{ \AA}$ and at $D \leq 50$ kpc for CGM gas with $W_r(2796) \geq 1.0 \text{ \AA}$. There is no clear difference between the covering fraction profile of blue galaxies versus red galaxies within 100 kpc, though the gas in red galaxies may be more concentrated near the center of the galaxy than in blue galaxies. Outside 100 kpc, red galaxies have smaller covering fractions than blue galaxies and no absorption for $W_r(2796) \geq 0.6$. The high redshift galaxies ($z \geq \langle z \rangle$) have a higher covering fraction than the low redshift galaxies ($z < \langle z \rangle$) at $D > 50$ kpc.

5. We determined the best-fit parameters R_* and β for the luminosity scaling of the outer envelope for absorption, or the “halo absorption radius”, $R(L) = R_*(L/L^*)^\beta$, for both the B - and K -bands as a function of $W_r(2796)$ threshold. For the B -band, the luminosity scaling increases from $\beta \sim 0.3$ to $\beta \sim 0.4$ with increasing W_{cut} . We find $R_* \sim 80$ kpc for $W_{\text{cut}} = 0.1$ and 0.3 \AA , and $R_* \sim 75$ kpc for $W_{\text{cut}} = 0.6$ and 1.0 \AA . The covering fraction inside $R(L_B)$ decreases from $f_{R(L)} = 0.85$ for $W_{\text{cut}} = 0.1 \text{ \AA}$ to $f_{R(L)} = 0.34$ for $W_{\text{cut}} = 1.0 \text{ \AA}$. For the K -band, the luminosity scaling ranges from $\beta \sim 0.2$ to 0.3 , and R_* ranges from ~ 60 kpc to ~ 80 kpc. The covering fraction behaves similarly to the B -band. Though the “outer envelope” for absorption has a clear dependence on both luminosity and $W_r(2796)$ threshold, we note that the scatter in the data in the $W_r(2796)$ - D plane, the behavior of the covering fraction profile $f_{(D)}$ with increasing D , and the relatively extended upward uncertainties in R^* all indicate that $R(L)$ is not a well-defined quantity, but should be interpreted as a “fuzzy” boundary and that the “fuzziness” increases with decreasing equivalent width threshold.

6. Dividing the galaxies by the median color ($B-K = 1.48$), adopting $W_{\text{cut}} = 0.3 \text{ \AA}$, and examining the fit parameters to $R(L) = R_*(L/L^*)^\beta$, we find that red galaxies have a steeper luminosity scaling, β , and larger halo absorption radii, R_* , than blue galaxies in both the B - and K -bands. This behavior of larger R_* for red galaxies is consistent with the results of Bordoloi et al. (2011), though our values are smaller. Using the K -band as a proxy for stellar mass, we may be seeing that the difference in the values of R_* and β between red and blue galaxies is due to the mass of a galaxy such that more massive galaxies have larger halo absorption radii (also see

Churchill et al. 2013c).

7. We also examined the $R(L)$ dependence in both the B - and K -bands on galaxy redshift, slicing the sample at the median redshift $z = 0.359$, and adopting $W_{\text{cut}} = 0.3 \text{ \AA}$. In the B -band, we find $R_* \sim 80$ kpc, $\beta \sim 0.4$, and $f_{R(L)} \sim 0.8$ in the low z subsample. The high z subsample has similar values for R_* (~ 85 kpc) and $f_{R(L)}$ (~ 0.8), but a much shallower dependence on L_B/L_B^* , with $\beta \sim 0.3$. In the K -band, we find no discernible difference within uncertainties between the low and high z subsamples. The values for R_* , β , and $f_{R(L)}$ for both subsamples are ~ 80 kpc, ~ 0.3 , and ~ 0.8 , respectively.

This work constitutes our first examination of the relationship of the MgII absorbing CGM with galaxy properties using MAGIIICAT. In particular, we have examined the data by comparing direct observables and have avoided analyzing the quantities based upon converting or scaling the data to a preferred model of the CGM. Our aim has been to provide an unfiltered view of the Mg II absorbing CGM. Nonetheless, the simple bivariate testing we have conducted here does not provide full leverage for probing of the available data. In future work, we will apply multivariate analysis methods in which we also incorporate mass estimates of the galaxies, Mg II kinematics, and both low and high ionization absorption strengths of the CGM for these galaxies. We will also conduct comparative studies of the isolated galaxies and group galaxies in the catalog.

We thank the anonymous referee for a careful reading of the manuscript and for valuable input that improved this work. We also thank Nick Gnedin for reading and providing insightful comments on an earlier draft. This research was primarily supported through grant HST-AR-12646 provided by NASA via the Space Telescope Science Institute, which is operated by the Association of Universities for Research in Astronomy (AURA) under NASA contract NAS 5-26555. This work was also supported by the Research Enhancement Program provided by NASA’s New Mexico Space Grant Consortium (NMSGC). NMN was also partially supported through a NMSGC Graduate Fellowship and a three-year Graduate Research Enhancement Grant (GREG) sponsored by the Office of the Vice President for Research at New Mexico State University.

REFERENCES

- Adelberger, K. L., Shapley, A. E., Steidel, C. C., et al. 2005, *ApJ*, 629, 636
 Barton, E. J., & Cooke, J. 2009, *AJ*, 138, 1817
 Bechtold, J., & Ellingson, E. 1992, *ApJ*, 396, 20
 Benjamin, R. A., & Danly, L. 1997, *ApJ*, 481, 764
 Bergeron, J., & Boissè, P. 1991, *A&A*, 243, 334
 Bergeron, J., & Stasińska, G. 1986, *A&A*, 169, 1
 Birboim, Y., & Dekel, A. 2003, *MNRAS*, 345, 349
 Birboim, Y., Dekel, A., & Neistein, E. 2007, *MNRAS*, 380, 339
 Bolzonella, M., Miralles, J.-M., & Pelló, R. 2000, *A&A*, 363, 476
 Bordoloi, R., Lilly, S. J., Knobel, C., et al. 2011, *ApJ*, 743, 10
 Bouché, N., Hohensee, W., Vargas, R., et al. 2012, *MNRAS*, 426, 801
 Bouché, N., Murphy, M. T., Péroux, C., Csabai, I., & Wild, V. 2006, *MNRAS*, 371, 495
 Brown, B. W., Hollander, M., & Korwar, R. M. 1974, in *Reliability and Biometry*, 327
 Bruzual A. G., & Charlot, S. 1993, *ApJ*, 405, 538
 Charlton, J. C., & Churchill, C. W. 1996, *ApJ*, 465, 631
 Chelouche, D., & Bowen, D. V. 2010, *ApJ*, 722, 1821
 Ceverino, D., & Klypin, A. 2009, *ApJ*, 695, 292
 Charlton, J. C., & Churchill, C. W. 1998, *ApJ*, 499, 181
 Chen, H.-W., Helsby, J. E., Gauthier, J.-R., Sheckman, S. A., Thompson, I. B., & Tinker, J. L. 2010a, *ApJ*, 714, 1521
 Chen, H.-W., Lanzetta, K. M., & Webb, J. K. 2001a, *ApJ*, 556, 158
 Chen, H.-W., Lanzetta, K. M., Webb, J. K., & Barcons, X. 2001b, *ApJ*, 559, 654
 Chen, H.-W., Wild, V., Tinker, J. L., et al. 2010b, *ApJ*, 724, L176
 Chen, H.-W., & Tinker, J. L. 2008, *ApJ*, 687, 745
 Churchill, C. W., Kacprzak, G. G., Nielsen, N. M., Steidel, C. C., Murphy, M. T. 2013a, *ApJ*, submitted
 Churchill, C. W., Kacprzak, G. G., & Steidel, C. C. 2005, *IAU Colloq.* 199: Probing Galaxies through Quasar Absorption Lines, 24
 Churchill, C. W., Kacprzak, G. G., Steidel, C. C., & Evans, J. L. 2007, *ApJ*, 661, 714
 Churchill, C. W., Mellon, R. R., Charlton, J. C., Jannuzi, B. T., Kirhakos, S., Steidel, C. C., & Schneider, D. P. 2000a, *ApJS*, 130, 91
 Churchill, C. W., Mellon, R. R., Charlton, J. C., et al. 2000b, *ApJ*, 543, 577
 Churchill, C. W., Nielsen, N. M., Kacprzak, G. G., & Trujillo-Gomez, S. 2013b, *ApJ*, 763, L42
 Churchill, C. W., Rigby, J. R., Charlton, J. C., & Vogt, S. S. 1999, *ApJS*, 120, 51
 Churchill, C. W., Steidel, C. C., & Vogt, S. S. 1996, *ApJ*, 471, 164
 Churchill, C. W., Trujillo-Gomez, S., Nielsen, N. M., & Kacprzak, G. G. 2013c, *ApJ*, submitted
 Churchill, C. W., & Vogt, S. S. 2001, *AJ*, 122, 679
 Churchill, C. W., Vogt, S. S., & Charlton, J. C. 2003, *AJ*, 125, 98

- Cirasuolo, M., McLure, R. J., Dunlop, J. S., Almaini, O., Foucaud, S., & Simpson, C. 2010, *MNRAS*, 401, 1166
- Coleman, G. D., Wu, C.-C., & Weedman, D. W. 1980, *ApJS*, 43, 393
- Dekel, A., & Birnboim, Y. 2006, *MNRAS*, 368, 2
- Dekel, A., & Silk, J. 1986, *ApJ*, 303, 39
- Evans, J. L. 2011, Ph.D. Thesis, New Mexico State University
- Faber, S. M., et al. 2007, *ApJ*, 665, 265
- Fried, J. W., von Kuhlmann, B., Meisenheimer, K., et al. 2001, *A&A*, 367, 788
- Gauthier, J.-R., Chen, H.-W., & Tinker, J. L. 2009, *ApJ*, 702, 50
- Gehrels, N. 1986, *ApJ*, 303, 336
- Guillemin, P., & Bergeron, J. 1997, *A&A*, 328, 499
- Kacprzak, G. G., & Churchill, C. W. 2011a, *ApJ*, 743, L34
- Kacprzak, G. G., Churchill, C. W., Barton, E. J., & Cooke, J. 2011b, *ApJ*, 733, 105
- Kacprzak, G. G., Churchill, C. W., Ceverino, D., et al. 2010, *ApJ*, 711, 533
- Kacprzak, G. G., Churchill, C. W., Evans, J. L., Murphy, M. T., & Steidel, C. C. 2011c, *MNRAS*, 416, 3118
- Kacprzak, G. G., Churchill, C. W., & Nielsen, N. M. 2012, *ApJ*, 760, L7
- Kacprzak, G. G., Churchill, C. W., Steidel, C. C., & Murphy, M. T. 2008, *AJ*, 135, 922
- Kacprzak, G. G., Churchill, C. W., Steidel, C. C., Murphy, M. T., & Evans, J. L. 2007, *ApJ*, 662, 909
- Kacprzak, G. G., Churchill, C. W., Steidel, C. C., Spitler, L. R., & Holtzman, J. A. 2012, *MNRAS*, 427, 3029
- Kacprzak, G. G., Murphy, M. T., & Churchill, C. W. 2010, *MNRAS*, 406, 445
- Kereš, D., Katz, N., Fardal, M., Davé, R., & Weinberg, D. H. 2009, *MNRAS*, 395, 160
- Kereš, D., Katz, N., Weinberg, D. H., & Davé, R. 2005, *MNRAS*, 363, 2
- Kim, A., Goobar, A., & Perlmutter, S. 1996, *PASP*, 108, 190
- Lanzetta, K. M., & Bowen, D. 1990, *ApJ*, 357, 321
- Lanzetta, K. M., & Bowen, D. V. 1992, *ApJ*, 391, 48
- Lanzetta, K. M., Bowen, D. V., Tytler, D., & Webb, J. K. 1995, *ApJ*, 442, 538
- Le Brun, V., Bergeron, J., Boisse, P., & Christian, C. 1993, *A&A*, 279, 33
- Lehner, N., Howk, J. C., Tripp, T. M., et al. 2013, *ApJ*, 770, 138
- Lilly, S. J., Tresse, L., Hammer, F., Crampton, D., & Le Fevre, O. 1995, *ApJ*, 455, 108
- Lin, H., Yee, H. K. C., Carlberg, R. G., et al. 1999, *ApJ*, 518, 533
- Lundgren, B. F., Brunner, R. J., York, D. G., et al. 2009, *ApJ*, 698, 819
- Maller, A. H., & Bullock, J. S. 2004, *MNRAS*, 355, 694
- Martin, C. L., & Bouché, N. 2009, *ApJ*, 703, 1394
- McGuagh, S. S., Schombert, J. M., de Blok, W. J. G., & Zagursky, M. J. 2010, *ApJ*, 708, L14
- Ménard, B., Wild, V., Nestor, D., et al. 2011, *MNRAS*, 417, 801
- Mo, H. J., & Miralda-Escude, J. 1996, *ApJ*, 469, 589
- Narayanan, A., Misawa, T., Charlton, J. C., & Kim, T.-S. 2007, *ApJ*, 660, 1093
- Navarro, J. F., Frenk, C. S., & White, S. D. M. 1996, *ApJ*, 462, 563
- Nestor, D. B., Turnshek, D. A., & Rao, S. M. 2005, *ApJ*, 628, 637
- Nielsen, N. M., Churchill, C. W., Kacprzak, G. G., & Murphy, M. T. 2013, arXiv:1304.6716 (Paper I)
- Ocvirk, P., Pichon, C., Teyssier, R. 2008, *MNRAS*, 390, 1326
- Oppenheimer, B. D., Davé, R., Kereš, D., et al. 2010, *MNRAS*, 406, 2325
- Petitjean, P., & Bergeron, J. 1990, *A&A*, 231, 309
- Rao, S. M., & Turnshek, D. A. 2000, *ApJS*, 130, 1
- Ribaudo, J., Lehner, N., Howk, J. C., et al. 2011, *ApJ*, 743, 207
- Rigby, J. R., Charlton, J. C., & Churchill, C. W. 2002, *ApJ*, 565, 743
- Rubin, K. H. R., Prochaska, J. X., Koo, D. C., & Phillips, A. C. 2012, *ApJ*, 747, L26
- Rubin, K. H. R., Weiner, B. J., Koo, D. C., et al. 2010, *ApJ*, 719, 1503
- Rudie, G. C., Steidel, C. C., Trainor, R. F., et al. 2012, *ApJ*, 750, 67
- Schneider, D. P., et al. 1993, *ApJS*, 87, 45
- Simcoe, R. A., Sargent, W. L. W., Rauch, M., & Becker, G. 2006, *ApJ*, 637, 648
- Steidel, C. C. 1995, *QSO Absorption Lines*, 139
- Steidel, C. C., Dickinson, M., Meyer, D. M., Adelberger, K. L., & Sembach, K. R. 1997, *ApJ*, 480, 586
- Steidel, C. C., Dickinson, M., & Persson, S. E. 1994, *ApJ*, 437, L75
- Steidel, C. C., Erb, D. K., Shapley, A. E., et al. 2010, *ApJ*, 717, 289
- Steidel, C. C., & Sargent, W. L. W. 1992, *ApJS*, 80, 1
- Stewart, K. R., Kaufmann, T., Bullock, J. S., et al. 2011, *ApJ*, 738, 39
- Tinker, J. L., & Chen, H.-W. 2008, *ApJ*, 679, 1218
- Thom, C., Werk, J. K., Tumlinson, J., et al. 2011, *ApJ*, 736, 1
- Tremonti, C. A., Moustakas, J., & Diamond-Stanic, A. M. 2007, *ApJ*, 663, L77
- Tripp, T. M., & Bowen, D. V. 2005, *IAU Colloq. 199: Probing Galaxies through Quasar Absorption Lines*, 5
- Tumlinson, J., Thom, C., Werk, J. K., et al. 2011, *Science*, 334, 948
- Turnshek, D. A., Rao, S. M., Nestor, D. B., Belfort-Mihalyi, M., & Quider, A. M. 2005, *IAU Colloq. 199: Probing Galaxies through Quasar Absorption Lines*, 104
- van de Voort, F., Schaye, J., Booth, C. M., Haas, M. R., & Dalla Vecchia, C. 2011, *MNRAS*, 414, 2458
- van de Voort, F., & Schaye, J. 2012, *MNRAS*, 423, 2991
- Wang, W., & Wells, M. T. 2000, *Statistica Sinica*, 10, 1199
- Weiner, B. J., Coil, A. L., Prochaska, J. X., et al. 2009, *ApJ*, 692, 187
- Weisheit, J. C. 1978, *ApJ*, 219, 829
- Wolf, C., Meisenheimer, K., Rix, H.-W., et al. 2003, *A&A*, 401, 73
- Wolynetz, M. S. 1979, *Journal of the Royal Statistical Society*, 28, 195
- Yanny, B., & York, D. G. 1992, *ApJ*, 391, 569
- Zibetti, S., Ménard, B., Nestor, D. B., Quider, A. M., Rao, S. M., & Turnshek, D. A. 2007, *ApJ*, 658, 161